Constitutive $P2Y_2$ receptor activity regulates basal lipolysis in human adipocytes

Seema B. Ali[1], Jeremy J. O. Turner[2] and Samuel J. Fountain[1,3]

[1] Biomedical Research Centre, School of Biological Sciences, University of East Anglia, Norwich, UK
[2] Norfolk & Norwich University Hospital, Colney Lane, Norwich, UK
[3] Corresponding author: Email s.j.fountain@uea.ac.uk

Keywords: Adipose tissue, Purinergic receptor, Calcium signalling, Human

Conflict of interest statement

No competing interests declared.

Summary statement

Basal lipolysis and adipokine secretion are controlled by autocrine purinergic signaling via $P2Y_2$ receptors in human adipocytes.

JCS Advance Online Article. Posted on 17 October 2018

ABSTRACT

White adipocytes are key regulators of metabolic homeostasis, which release stored energy as free fatty acids via lipolysis. Adipocytes possess both basal and stimulated lipolytic capacity, but limited information exists regarding the molecular mechanisms that regulate basal lipolysis. Here, we describe a mechanism whereby autocrine purinergic signaling and constitutive $P2Y_2$ receptor activation suppresses basal lipolysis in primary human *in vitro* differentiated adipocytes. We found that human adipocytes possess cytoplasmic calcium tone due to ATP secretion and constitutive $P2Y_2$ receptor activation. Pharmacological antagonism or knockdown of $P2Y_2$ receptors increases intracellular cAMP levels and enhances basal lipolysis. $P2Y_2$ receptor antagonism works synergistically with phosphodiesterase inhibitors in elevating basal lipolysis, but is dependent upon adenylate cyclase activity. Mechanistically, we suggest that the increased calcium tone exerts an anti-lipolytic effect by suppression of calcium-sensitive adenylate cyclase isoforms. We also observed that acute enhancement of basal lipolysis following $P2Y_2$ receptor antagonism alters the profile of secreted adipokines leading to longer term adaptive decreases in basal lipolysis. Our findings reveal that basal lipolysis and adipokine secretion are controlled by autocrine purinergic signaling in human adipocytes.

INTRODUCTION

White adipose tissue (WAT) is the primary site of long-term energy storage within mammals. WAT comprises of a diverse range of cells, of which the predominant cell type is white adipocytes. White adipocytes play a pivotal role in the endocrine function of WAT via the production and release of adipokines to regulate systemic metabolism (Halberg et al. 2008). However, their primary function is to facilitate long-term storage of excess nutrients within large lipid droplets. These lipid droplets give white adipocytes their distinctive unilocular morphology. Adipocytes are highly dynamic cells, which store excess energy in the form of triglycerides in the fed state via lipogenesis and release energy in the form of free fatty acids during fasting via lipolysis (Rutkowski et al. 2015). The metabolic activity of white adipocytes is regulated tightly by hormones and the autonomic nervous system to achieve whole body metabolic homeostasis. As such, loss of adipocyte control is associated with cardiovascular risk and obesity (Nielsen et al. 2014; Rosen & Spiegelman 2006). Adipocytes possess both a basal and stimulated lipolytic capacity. The most well characterised stimulated lipolytic pathway is mediated by sympathetic nerve stimulation of WAT via β-adrenoreceptors. Upon

activation of β-adrenoreceptors, G_s-mediated stimulation of adenylate cyclase is initiated, which causes an elevation in cytoplasmic cyclic AMP. Subsequently, this activates protein kinase A, which in turn phosphorylates hormone sensitive lipase (HSL) and perilipins on the surface of the lipid droplet to allow translocation of HSL to the lipid droplet (Miyoshi et al. 2006), where HSL, in combination with adipose triglyceride lipase (ATGL) and monoglyceride lipase (MGL), catalyses the hydrolysis of triglycerides to free fatty acids and glycerol molecules. The free fatty acids can then be released into the bloodstream where they are able to travel to distant organs and be utilised as a cellular energy source (Ahmadian et al. 2010). Despite the importance of basal lipolysis in regulating adipose tissue volume and the level of circulating free fatty acids (Heckmann et al. 2014; Miyoshi et al. 2008; Rydén & Arner 2017), the molecular mechanisms regulating basal lipolysis are less well defined than the stimulated lipolytic pathways.

The concentration of free cytoplasmic Ca^{2+} and the rhythmicity of Ca^{2+} oscillations within the cytoplasm, are critical regulators of many important processes within mammalian cells, including gene expression, cytoskeletal rearrangement, secretion and metabolism (Clapham 2007). In adipocytes, intracellular Ca^{2+} is known to be a key regulator of adipocyte differentiation (Shi et al. 2000) and metabolism (Arruda & Hotamisligil 2015), but cell surface receptors that evoke intracellular Ca^{2+} responses and how they are linked to metabolic control of human adipocytes are poorly defined.

Adipocytes in white adipose tissue are innervated by the sympathetic branch of the autonomic nervous system (Bartness et al. 2014). Increased sympathetic tone drives lipolysis through the action of noradrenaline on β-adrenergic receptors expressed at the adipocyte cell surface (Ahmadian et al. 2010). Consequently, local denervation of white adipose depots in pre-clinical models leads to fat pad expansion (Bowers et al. 2004). Sympathetic neurons release ATP as a co-transmitter with noradrenaline during innervation of a range of tissues (Kennedy 2015). In addition, ATP is also released physiologically by cells during inflammation and injury where it acts as a danger-associated molecular pattern (Gorini et al. 2013). We and others have also documented constitutive release of ATP by differing mammalian cell types (Corriden & Insel 2010; Sivaramakrishnan et al. 2012), which produces a resting steady concentration of ATP close to the cell surface and tonic activation of some purinergic receptor subtypes. Extracellular ATP can evoke changes in cytoplasmic Ca^{2+} via activation of P2X and P2Y cell surface

purinergic receptors. P2X receptors ($P2X_{1\text{-}7}$) are non-selective ligand-gated ion channels activated by extracellular ATP that are directly permeate to Ca^{2+} (North 2002). P2Y receptors ($P2Y_{1,2,4,6,11,12,13\text{ and }14}$) are G protein-coupled receptors that are activated by ATP, ADP, UTP, UDP and UDP-sugars in a subtype-specific fashion (von Kügelgen & Hoffmann 2016). $P2Y_{1,2,4,6\text{ and }11}$ are G_q-coupled receptors, so upon activation they elevate cytoplasmic Ca^{2+} through IP_3-mediated release of Ca^{2+} stored in the endoplasmic reticulum. $P2Y_{13}$ and $P2Y_{14}$ receptors are G_i-coupled and evoke pertussis-toxin sensitive intracellular Ca^{2+} responses. $P2Y_{12}$ receptors are also G_i-coupled, but do not evoke intracellular Ca^{2+} responses, instead they positively regulate intracellular Ca^{2+} responses evoked by other P2Y receptors (Micklewright et al. 2018). The repertoire and function of cell surface purinergic receptors expressed by human adipocytes is currently unclear. Here we sought to determine what purinergic receptors are expressed by primary human *in vitro* differentiated adipocytes and investigate their potential in regulating basal lipolysis.

RESULTS

ATP, ADP and UTP-evoked intracellular Ca^{2+} responses in human adipocytes

A representative image of human adipose-derived mesenchymal stromal cells differentiated to mature adipocytes following the habituation protocol is shown in **Fig 1A**. Application of exogenous ATP, ADP and UTP evoked intracellular Ca^{2+} responses in adipocytes (**Fig 1B)** with a rank order of potency of ADP (EC_{50} 239 ± 48.1 nM; *N*=6) > ATP (EC_{50} 1.84 ± 1.42 μM; *N*=6) > UTP (EC_{50} 13.0 ± 4.6 μM; *N*=6) (**Fig 1C**). The magnitude of the responses at maximal agonist concentrations also had the rank order of ADP > ATP > UTP (**Fig 1D**). *In vitro* differentiated adipocytes were unresponsive to UDP (<30 μM) and UDP-glucose (<100 μM) (*N*=6) (data not shown).

ATP responses were metabotropic in nature as responses persisted in the absence of extracellular Ca^{2+} (**Figs 1E,F**), but were abolished following phospholipase C inhibition with U73122 (**Figs 1G,H**). However, the responses to ATP decreased in the absence of extracellular calcium, which suggests that extracellular calcium is important for the magnitude of the response. We next used selective receptor antagonists to probe the molecular basis of nucleotide-evoked Ca^{2+} responses in human adipocytes. ATP-evoked responses were attenuated following selective antagonism of $P2Y_1$, $P2Y_2$ and $P2Y_{12}$ receptors with MRS2500 (IC_{50} 415 ± 160 nM; *N*=6), AR-C118925XX (IC_{50} 683 ± 116 nM; *N*=6) and PSB-0739 (IC_{50} >

10μM; *N*=6), respectively (**Table S1, Figs 2A-D**). The responses could be inhibited further by combining $P2Y_1$, $P2Y_2$ and $P2Y_{12}$ selective antagonists (**Fig 2E**), suggesting that in addition to the ATP/UTP-activated $P2Y_2$ receptor, ADP-activated receptors $P2Y_1$ and $P2Y_{12}$ actively contribute to the ATP response. This is likely to be due to ectonucleotidase breakdown of extracellular ATP to ADP (Yegutkin 2008). Contribution of $P2Y_1$ receptors to the ATP/ADP response is expected due to its G_q coupling, however the contribution of the G_i-coupled $P2Y_{12}$ receptor is less expected, though not unprecedented as it has been shown in other cell types (Micklewright et al., 2018). In addition, $P2Y_1$ (MRS2500; IC_{50} 77.1 ± 37.5 nM; *N*=6) or $P2Y_{12}$ (PSB-0739; IC_{50} 64.0 ± 56.5 nM; *N*=6) receptor antagonism attenuated ADP-evoked Ca^{2+} signalling in adipocytes (**Figs 2F,H**), with further attenuation observed when the antagonists were combined (**Fig 2I**). A role for $P2Y_{12}$ and G_i-coupling was further substantiated as pertussis toxin, an inhibitor of G_i-signalling (Katada et al. 1983), inhibited both the ATP and ADP-evoked intracellular Ca^{2+} responses in human adipocytes (**Figs 2J,K**).

P2Y receptor expression in human adipocytes and human adipose tissue

Analysis by quantitative RT-PCR revealed a diverse expression profile of purinergic receptors in human adipocytes, including $P2X_{4\text{-}7}$, $P2Y_1$, $P2Y_2$, $P2Y_4$, $P2Y_6$, $P2Y_{11}$, $P2Y_{12}$ and $P2Y_{13}$, whereas $P2X_1$, $P2X_2$, $P2X_3$ and $P2Y_{14}$ are not expressed (**Fig 3A**). The same receptor subtypes were detected by immunocytochemistry in adipocytes *in vitro* (**Fig 3B**). The expression of $P2Y_1$, $P2Y_2$ and $P2Y_{12}$ is supported by the functional pharmacology presented (**Fig 2**). However, despite detection at the mRNA and protein level, the use of selective antagonists for $P2X_4$ (≤ 30 μM PSB12062), $P2X_7$ (≤ 10 μM A438079), $P2Y_6$ (≤ 10 μM MRS2578), $P2Y_{11}$ (≤ 10 μM NF340) and $P2Y_{13}$ (≤ 3 μM MRS2211) had no effect on ATP and/or ADP-evoked intracellular Ca^{2+} responses in adipocytes (**Table S1**) suggesting these subtypes are not involved under the conditions tested. $P2Y_1$, $P2Y_2$ and $P2Y_{12}$ expression was also confirmed in adipocytes in sections of human subcutaneous adipose tissue (**Fig 3C**).

Constitutive $P2Y_2$ receptor activity produces intracellular Ca^{2+} tone

Extracellular ATP is known to act both as a paracrine and autocrine signal, and we and others have previously observed some mammalian cells to have a halo of extracellular ATP due to constitutive release (Corriden & Insel 2010; Sivaramakrishnan et al. 2012). To this end, we sought to investigate the ability of human adipocytes to secrete ATP and the impact this has on homeostasis. Bulk phase luminometry measurements of ATP revealed the ability of human adipocytes to condition the culture medium with approximately 50nM ATP (**Fig 4A**), which is

likely to be an underestimation of the acutely pericellular ATP concentration. Scavenging extracellular ATP with apyrase caused a reduction in the resting level of cytoplasmic Ca^{2+} in human adipocytes (**Fig 4B**). These data suggest that extracellular ATP generates intracellular Ca^{2+} tone in human adipocytes, so we explored this further by investigating whether constitutive activity of $P2Y_1$, $P2Y_2$ and $P2Y_{12}$ receptors contribute to resting cytoplasmic Ca^{2+} levels. There was some variability in the resting cytoplasmic Ca^{2+} concentration between donors, as well as in the presence of different vehicle controls (water or 0.1% DMSO), however pairwise comparisons of the effect of each antagonist versus their respective vehicle control revealed that antagonism of either $P2Y_1$ or $P2Y_{12}$ had no significant effect of resting cytoplasmic Ca^{2+} (**Fig 4C,E**). However, a marked significant reduction was observed following selective $P2Y_2$ receptor antagonism (**Fig 4D**). In these experiments, resting cytoplasmic Ca^{2+} was reduced from approximately 125 nM to 50 nM free Ca^{2+}, suggesting that constitutive $P2Y_2$ activity, but not $P2Y_1$ or $P2Y_{12}$, generates intracellular Ca^{2+} tone in human adipocytes.

Constitutive $P2Y_2$ receptor activity suppresses lipolysis via an adenylate cyclase-dependent mechanism

The lipolytic activity of adipocytes that produces free fatty acids and glycerol is under hormonal and nervous control, but also occurs in the absence of lipolytic stimuli (basal lipolysis). Basal lipolysis in adipocytes was measured as a time-dependent conditioning of culture medium with glycerol in the absence of stimulation. Under these conditions, adipocytes freely released glycerol over a three-hour period (**Fig 5**). $P2Y_2$ receptor antagonism caused a significant increase in the rate of glycerol release, enhancing release by approximately 40% after 3 hours (**Fig 5A**). By comparison, stimulation of adipocytes with EC_{50} concentrations of isoprenaline (75 nM) to mimic nervous stimulation causes a 122 ± 24% (N=3) increase in glycerol release versus basal conditions. The $P2Y_2$ receptor antagonist AR-C118925XX enhanced basal glycerol release in a concentration-dependent fashion (**Fig 5B**). To further investigate the mechanism by which $P2Y_2$ antagonism increases basal lipolysis we quantified cellular cyclic AMP (cAMP), a positive effector of lipolysis in adipocytes, with and without AR-C118925XX treatment. AR-C118925XX treatment significantly elevated cellular cAMP in adipocytes (**Fig 5C**). To support these findings, we used lentivirus delivery of shRNA to knockdown $P2Y_2$ receptor expression in adipocytes to investigate the impact on lipolysis and intracellular cAMP levels. Using this strategy $P2Y_2$ mRNA could be knocked down by 59.8±3.7% (N=5; P<0.05) versus scrambled counterparts. The rate of basal lipolysis (**Fig 5D**)

and intracellular cAMP levels (**Fig 5E**) were both elevated in the $P2Y_2$ knockdown cells versus their scrambled counterparts. Interestingly, $P2Y_2$ knockdown adipocytes produced a small lipid droplet phenotype compared to their scrambled counterparts (**Fig 5F**), and the number of droplets per cell was significantly increased (**Fig 5G**). Such phenotypic changes in lipid droplets is associated with increased lipid metabolism (Paar et al., 2012). To this end, we quantified the amount of neutral lipid stored within scrambled and $P2Y_2$ knockdown adipocytes using BODIPY fluorescence, and demonstrated that $P2Y_2$ knockdown cells contained less neutral lipid (**Fig 5H**). Taken together these data suggest that reducing $P2Y_2$ activity by means of pharmacological antagonism or gene knockdown increases basal lipolysis in human adipocytes. In control experiments, antagonism of either $P2Y_1$ (**Fig 5I**) or $P2Y_{12}$ (**Fig 5J**) did not affect the rate of basal lipolysis, which is in line with a lack of effect on resting cytoplasmic Ca^{2+} (**Fig 4**).

To further understand how inhibition of constitutive $P2Y_2$ receptor activity leads to an increase in cAMP and basal lipolysis, we examined the dependency of these effects on the activity of phosphodiesterases (PDE) and adenylate cyclase. An elevation in intracellular Ca^{2+} is known to produce an anti-lipolytic effect in adipocytes, which has previously been ascribed to activation of Ca^{2+}-sensitive PDE subtypes (Xue et al. 2001). If the underlying mechanism through which inhibition of constitutive $P2Y_2$ activity leads to increased intracellular cAMP and enhanced lipolysis is via reducing cytoplasmic Ca^{2+} and PDE activity, it would be expected that enhanced lipolysis produced by $P2Y_2$ antagonism would be abolished by PDE inhibition. The pan-PDE inhibitor IBMX increased basal lipolysis to a level comparable to that of AR-C118925XX (**Fig 6A**). In addition, using subtype-specific antagonists we observed that inhibition of PDE3 (cilostamide) and PDE4 (rolipram), but not PDE1 (vinpocetine), PDE2 (PF-05180999) or PDE7 (BRL50481), increased basal lipolysis (**Fig 6A**). Cilostamide enhanced lipolysis to a level beyond that of rolipram, and is consistent with a dominant role of PDE3 in human adipocytes (Snyder et al. 2005). Combining AR-C118925XX with either cilostamide or rolipram produced a synergistic enhancement of basal lipolysis (**Fig 6A**), suggesting the effect of $P2Y_2$ antagonism on basal lipolysis is not dependent on the activity of either PDE3 or PDE4. Therefore, we looked for an alternative mechanism and explored the dependency of adenylate cyclase itself in mediating the effects of $P2Y_2$ antagonism on cAMP and basal lipolysis. By RT-PCR analysis, we identified that human adipocytes express adenylate cyclase isoforms 1, 2, 3, 4, 5, 6, 7 and 8, but not 9 (**Fig 6B**). Of these isoforms 5 and 6 are negatively regulated by cytoplasmic Ca^{2+} (Halls & Cooper 2011) and can be selectively inhibited over

other isoforms by low concentrations of SQ22,536 (<10 µM) (Brand et al. 2013). Under these conditions, 1µM SQ22536 had no significant effect on basal lipolysis (**Fig 6C**), consistent with tonic suppression of adenylate cyclase, but 1µM SQ22536 could inhibit the ability of $P2Y_2$ antagonism, with AR-C118925XX, to enhance basal lipolysis in adipocytes (**Fig 6C**). These data suggest that the effects of $P2Y_2$ antagonism on basal lipolysis are due to activation of Ca^{2+}-sensitive isoforms of adenylate cyclase.

Pharmacological antagonism of $P2Y_2$ leads to acute enhancement of lipolysis. However, we observed that the rate of basal lipolysis is diminished after 24 hours following AR-C118925XX treatment compared to counterpart cells treated with vehicle control (**Fig 7A**). We reasoned that the increase in basal lipolysis may give rise to initiation of a negative feedback effect due to the enhanced secretion of adipokines with anti-lipolytic activity. To this end, we investigated the impact of pharmacological manipulation of constitutive $P2Y_2$ activity on the profile of secreted adipokines in human adipocytes. Analysis of secreted adipokines by protein array revealed changes in the profile of adipokines secreted in response to AR-C118925XX treatment (**Fig 7B and Table S2**). Of particular interest was the dramatically enhanced secretion of adipokines with anti-lipolytic activity including adiponectin (Qiao et al. 2011; Wedellová et al. 2011) and adipsin (Van Harmelen et al. 1999; Ronti et al. 2006), and the down-regulation of several adipokines that stimulate lipolysis including angiopoietin-like 4 (ANGPTL4) protein (Gray et al. 2012; La Paglia et al. 2017) and retinol-binding protein 4 (Lee et al. 2016) (**Fig 7C**).

DISCUSSION

This study has identified a diverse profile of purinergic receptors present in primary human adipocytes, however interestingly only $P2Y_1$, $P2Y_2$ and $P2Y_{12}$ receptors appear to be functionally involved in nucleotide-evoked calcium responses. Although $P2X_{4\text{-}7}$ receptors were detected at both the mRNA and protein level, the ATP response appears to be mediated by metabotropic P2Y receptors, as evidenced by the persistence of response in the absence of extracellular calcium, abolishment of the response when PLC was inhibited and no effect of selective antagonism of $P2X_4$ and $P2X_7$. $P2X_4$ receptors are known to localise to lysosomes and rapidly traffic to and from the plasma membrane in other cell types (Stokes 2013; Ashour & Deuchars 2004), which may explain why exogenous application of ATP was unable to activate $P2X_4$. A lack of involvement of $P2X_5$ and $P2X_6$ is unsurprising, as these receptors are not functional in humans (Torres et al. 1999; Ormond 2006; Kotnis et al. 2010). $P2X_7$ receptors

require very high concentrations of ATP to be activated (North 2002), so perhaps in this study, the concentration of ATP used was not sufficiently elevated to activate $P2X_7$. In addition, several P2Y receptor subtypes ($P2Y_4$, $P2Y_6$, $P2Y_{11}$ and $P2Y_{13}$) were also detected in human adipocytes, but do not appear to play a functional role in nucleotide-evoked calcium responses in these cells. In the case of $P2Y_4$, it is not possible to definitively rule out a role for this receptor, due to the absence of a commercially available selective antagonist for $P2Y_4$ (Jacobson et al. 2009). However, the observation that the response to UTP, the preferred agonist for $P2Y_4$, is abolished by selective antagonism of $P2Y_2$ indicates that $P2Y_4$ is unlikely to play a role in the UTP-evoked calcium response in human adipocytes. A possible explanation for the lack of involvement of $P2Y_4$, $P2Y_6$, $P2Y_{11}$ and $P2Y_{13}$ receptors is that $P2Y_2$ receptor activation caused heterologous desensitisation of these subtypes (Govindan & Taylor 2012). An important caveat to this study is that the Ca^{2+} responses reported are measurements from populations of adipocytes, and therefore variability of responses at the single cell level will be lost.

The $P2Y_2$ receptor is capable of sensing extracellular ATP in the nanomolar range (Lazarowski et al. 1995), thus the concentration of extracellular ATP released by adipocytes in this study is sufficient to activate $P2Y_2$. Here, we report that these properties of the $P2Y_2$ receptor allow it to be constitutively active due to the extracellular ATP microenvironment of human adipocytes. Furthermore, we provide data to demonstrate the functional importance of this constitutive activity in regulation of adipocyte intracellular Ca^{2+} tone, the rate of basal lipolysis and the profile of secreted adipokines. Though this is the first demonstration in human adipocytes, we and others have previously demonstrated the role purinergic receptors can play in autocrine regulation of mammalian cells due to constitutive or agonist-triggered ATP release (Corriden & Insel 2010; Sivaramakrishnan et al. 2012).

In this study, we contribute the acute anti-lipolytic activity of $P2Y_2$ antagonism to a decrease in resting cytoplasmic Ca^{2+}. Previous studies have highlighted an importance of free cytoplasmic Ca^{2+} in regulating lipolysis (Xue et al. 2001), though the molecular mechanisms underlying this are unclear. Certain PDE isoforms, specifically PDE1 isoforms, are sensitive to and activated by Ca^{2+} (Omori & Kotera 2007) via a Ca^{2+}/calmodulin-dependent mechanism. Stimulation of basal lipolysis following $P2Y_2$ antagonism could arise via this mechanism due to a decrease in cytoplasmic Ca^{2+} and the consequent loss of PDE activity, increasing the availability of cAMP and promoting lipolysis. However, our findings do not support this

mechanism as direct PDE inhibition has a synergistic effect with $P2Y_2$ antagonism on lipolysis. Furthermore, use of the vinpocetine, a selective inhibitor of Ca^{2+}/calmodulin-sensitive PDE1 isoforms, had no effect on basal lipolysis, suggesting PDE1 does not regulate basal lipolysis. As the stimulatory action of $P2Y_2$ receptor antagonism on basal lipolysis is completely inhibited by the adenylate cyclase inhibitor SQ22,536, we suggest the role of constitutively active $P2Y_2$ may be to directly control the activity of adenylate cyclase and acutely regulate lipolysis via this route. One interesting observation is that adenylate cyclase inhibition does not decrease basal lipolysis, which suggests that adenylate cyclase activity is tonically suppressed. This observation is consistent with findings in rodent adipocytes (Juan et al. 2005; Jun et al. 2006). Our model suggests that adenylate cyclase activity does not contribute to the basal lipolytic capacity of adipocytes due to tonic suppression by elevated cytoplasmic Ca^{2+} (**Fig 8**). However, basal lipolysis occurs even in the absence of adenylate cyclase activity or activation of hormone-sensitive lipase (HSL) via the cAMP/PKA signalling axis, which is a known and important mediator of hormone and nervous stimulated lipolysis. This may be explained by the existence of adipose triglyceride lipase (ATGL), which is a cAMP-independent lipase known to regulate basal lipolysis (Miyoshi et al. 2008; Wang et al. 2011).

The correlation between $P2Y_2$ receptor activity, elevated intracellular Ca^{2+}, cAMP reduction and lowered basal lipolysis, has lead us to the hypothesis that constitutive $P2Y_2$ activity suppresses adenylate cyclase activity (**Fig 8**). There is precedence for a role for adipocyte cytoplasmic Ca^{2+} tone in regulating adenylate cyclase activity, as several adenylate cyclase isoforms (types 5 and 6) are Ca^{2+}-sensitive (Cioffi et al. 2002). Type 6 in particular has been shown to be inhibited by Ca^{2+}-entry through store-operated channels, that are likely to be opened following $P2Y_2$ receptor activation. The molecular basis of some of these channels have recently been identified in mouse adipocytes, where they control adiponectin secretion (Sukumar et al. 2012).

Here we demonstrate that pharmacological inhibition of $P2Y_2$ has a biphasic effect on lipolysis, an acute stimulatory effect (within 3 hours) followed by a reduction in lipolysis after 24 hours. The consequent reduction may be the result of a change in the profile of secreted adipokines following $P2Y_2$ antagonism. Adipocytes can sense and autoregulate their lipolytic capacity through autocrine adipokine signalling. There is evidence for a local negative feedback loop between increased lipolysis and the release of adiponectin, whereby elevated free fatty acid concentrations promote adiponectin secretion (Bernstein et al. 2004; Krzyzanowska et al.

2007), which in turn acts on adipocytes to inhibit lipolysis (Qiao et al. 2011). There is a clear link between increased adipocyte metabolism and adipocyte inflammation (Greenberg & Obin 2006). In obesity the well documented recruitment of macrophages into adipose tissue and decreased insulin sensitivity is likely to underlie the enhanced basal lipolysis in inflamed adipose tissue (Weisberg et al. 2003), though some inflammatory cytokines also have acute actions on adipose function (Zhang et al. 2002). It is interesting therefore that antagonism of $P2Y_2$ leads to enhance secretion of several inflammatory cytokines including TGF-β and IL-8, and markers of acute phase inflammation including serum amyloid A and plasminogen activator inhibitor-1. Such factors may be secreted in response to the acute increase in lipolysis following AR-C118925XX treatment.

In summary, we provide evidence that constitutive $P2Y_2$ activity is important for the regulation of basal lipolysis. We also demonstrate that perturbations in its activity and consequent enhanced basal lipolysis alter the profile of secreted adipokines in human *in vitro* differentiated adipocytes. This study highlights the $P2Y_2$ receptor and microenvironmental ATP as novel targets for pharmacological manipulation of WAT function.

METHODS

Chemicals and reagents

All chemicals were purchased from Sigma-Aldrich (Dorset, UK) unless otherwise stated. Selective antagonists were obtained from Tocris Bioscience (Bristol, UK) ($P2Y_1$ MRS2500; $P2Y_2$ AR-C118925XX; $P2Y_6$ MRS2578; $P2Y_{11}$ NF340; $P2Y_{12}$ PSB-0739; $P2Y_{13}$ MRS2211; $P2X_4$ PSB12062; $P2X_7$ A438079; adenylate cyclase (SQ22,536) and G_i signalling (Pertussis toxin). U73122 (phospholipase C) was purchased from Santa Cruz Biotechnology (Texas, DA, USA). All isoform selective phosphodiesterase (PDE) inhibitors (PDE1 vinpocetine; PDE2 PF-05180999; PDE3 cilostamide; PDE4 rolipram; PDE7 BRL50481) were purchased from Sigma-Aldrich (Dorset, UK). Nucleotides were purchased from Abcam (Cambridge, UK), excluding ADP and UDP (Sigma-Aldrich, Dorset, UK).

Tissue donation

Subcutaneous abdominal adipose tissue samples were obtained from 48 healthy female volunteers, with an average age of 55.5 ± 1.5 (N=45, range 38-75), undergoing elective delayed deep inferior epigastric perforator flap operations. All recruited patients were prior breast

cancer sufferers who have had mastectomies as part of their cancer treatment and are now in remission. Recruited patients had an average body mass index (BMI) value of 27.7 ± 0.5 (*N*=34, range 24-35). Patients were normotensive with an average mean arterial pressure of 98.4 ± 1.6 (*N*=44). Samples were obtained with the assistance of the plastic surgery team at the Norfolk and Norwich University Hospital (NNUH). All volunteers were screened to exclude diabetics, patients with infections or cancer and patients on anti-inflammatory medication. Informed written consent was obtained from all volunteers prior to participation in the study. This study was ethically approved by the London-Stanmore Research Ethics Committee (152093) and the Research and Development department at the NNUH (2014EC03L).

Primary cell isolation from adipose tissue and *in vitro* differentiation

Primary cells were isolated from human subcutaneous adipose tissue using a slightly adapted form of standard isolation procedures (Turner et al. 2010). In brief, fresh adipose tissue samples were dissected to remove blood vessels, fibrous tissue and skin. The samples were then further minced and enzymatically digested with collagenase (type 1A) from *Clostridium histolyticum* (Sigma-Aldrich, Dorset, UK) and bovine pancreatic DNase I (Biomatik, Cambridge, Canada) for 30 minutes at 37ºC with regular mixing by inversion. The digested tissue samples were then passed through a 70 µm cell strainer and centrifuged for 5 minutes at 450 x *g*, which separated the sample into a floating fraction containing mature adipocytes and a pellet containing multipotent mesenchymal stromal cells (MSCs). The adipocytes were discarded and the MSCs were treated with a red cell lysis buffer, washed and then resuspended in culture media (DMEM supplemented with 4.5 g/L glucose, sodium pyruvate, L-glutamine, 10% FBS (v/v), 50 IU/ml penicillin and 50 µg/ml streptomycin) and left in a T175 flask overnight in a humidified incubator at 37ºC with 5% CO_2. The following day, the cells were washed twice with PBS to remove any non-adherent cells or debris and left in fresh serum-containing media until the cells were confluent, at which point they were trypsinised and seeded for experimental use. In this study, MSCs were plated at an initial seeding density of $2x10^4$ cells/well in 96 well plates, unless otherwise indicated. The cells were then allowed to grow to hyper-confluence over the next four days and then the differentiation protocol was initiated by removing the culture media and replacing it with differentiation media, which consisted of DMEM supplemented with 10% FBS, 50 IU/ml penicillin, 50 µg/ml streptomycin, 0.2 mM indomethacin, 1 µM dexamethasone, 0.5 mM 3-isobutyl-1-methylxanthine (IBMX) and 100 nM insulin, for 14 days. The differentiation media was replaced every four days. After two weeks, the differentiation media

was removed and exchanged back to culture media for a further three days before experimental use to allow the cells to habituate. In all instances where adipocytes are mentioned in this study, they are cells that have undergone the full *in vitro* differentiation and habituation protocol described. MSCs were passaged a maximum of four times for differentiation, although the majority of experiments were performed using cells from passage 1 and 2. Only cells that displayed >90% differentiated cells (as judged by eye) were deemed adequate for experimental use. All experiments were performed using cells from at least three independent donors.

Calcium mobilisation experiments

Culture media was aspirated off *in vitro* differentiated adipocytes and the cells were gently washed with salt buffered solution (SBS) (pH 7.4), containing 130 mM sodium chloride, 5 mM potassium chloride, 1.2 mM magnesium chloride, 1.5 mM calcium chloride, 8 mM D-(+)-glucose and 10 mM HEPES. The cells were then loaded with 2 μM Fura-2AM (Abcam, Cambridge, UK) in SBS supplemented with 0.01% (w/v) pluronic for 1 hour at 37ºC while being protected from light. The loading buffer was then removed and the cells were washed twice with SBS. Where applicable, the cells were incubated for a further 30 minutes with vehicle/ antagonists or calcium-free SBS (SBS lacking 1.5 mM calcium chloride, but containing 2 mM EGTA, pH 7.4). For pertussis toxin experiments, the pertussis toxin was added to the culture media 4 hours prior to commencing the calcium mobilisation experiments. All antagonists were dissolved in water or DMSO and were then further diluted in SBS, so that a final concentration of 0.1% DMSO was not exceeded, excluding U73122 and MRS2578 which required a final concentration of 1% DMSO. Finally, the cells were maintained at 37ºC and challenged with nucleotides administered by a FlexStation III microplate reader (Molecular Devices, San Jose, CA, USA), which also recorded the fluorescence (excitation 340 nm and 380 nm, emission 510 nm) every three seconds to provide fluorescence ratio (F_{ratio}) values. F_{ratio} values at every time point, peak F ratios and area under the curve data were extracted using SoftMax Pro 5.4.5 (Molecular Devices, San Jose, CA, USA) software.

Calcium calibration

In vitro differentiated adipocytes were loaded with Fura-2AM as per the calcium mobilisation experiment protocol and then incubated with SBS or Ca^{2+} free SBS for 30 minutes at 37ºC prior to challenging the cells with 2 μM ionomycin and recording the changes in intracellular calcium levels using a Flexstation III microplate reader. The Grynkiewicz formula

(Grynkiewicz et al. 1985) was then utilised to convert F_{ratio} values from calcium mobilisation assays to intracellular calcium concentrations. The Grynkiewicz formula is as follows:

$$[Ca^{2+}]_i = K_D \times \beta \times (R-R_{min})/(R_{max}-R)$$

Where K_D is the K_D for Fura2-AM at 37ºC which is 224 nM, β is the maximum fluorescence intensity at 380 nm for ionomycin in the absence of calcium divided by the minimum fluorescence at 380 nm for ionomycin in the presence of calcium, R_{min} is the minimum F_{ratio} value for ionomycin in absence of calcium and R_{max} is the maximum F_{ratio} value for ionomycin in the presence of calcium and R is the F_{ratio} value that needs to be converted. β, R_{max} and R_{min} were calculated by averaging the data from three independent donors.

Immunocytochemistry

MSCs were seeded onto glass coverslips and differentiated *in vitro*. All subsequent steps were conducted at room temperature unless otherwise stated. Culture media was gently aspirated off the cells and the cells were washed with PBS, fixed with 4% paraformaldehyde for 15 minutes and then permeabilised with 0.25% Triton X-100 for 10 minutes. Non-specific binding was blocked with 1% bovine serum albumin (BSA) and then the cells were incubated with the appropriate primary antibody (1:200) overnight at 4ºC. Primary antibodies were purchased from Santa Cruz Biotechnology (Dallas, TX, USA) (P2X5 Santa Cruz Biotechnology Cat# sc-15192, RRID:AB_2158092), $P2Y_{12}$ (Santa Cruz Biotechnology Cat# sc-27152, RRID:AB_2155964)), Alomone Labs (Jerusalem, Israel) (P2X4, Alomone Labs Cat# APR-002, RRID:AB_2040058; P2X7, Alomone Labs Cat# APR-004, RRID:AB_2040068; $P2Y_1$, Alomone Labs Cat# APR-009, RRID:AB_2040070; $P2Y_4$, Alomone Labs Cat# APR-006, RRID:AB_2040080; $P2Y_6$, Alomone Labs Cat# APR-011, RRID:AB_2040082; $P2Y_{11}$, APR-015; $P2Y_{13}$ Alomone Labs Cat# APR-015, RRID:AB_2040072) and abcam (Cambridge, UK) ($P2Y_2$, Abcam Cat# ab10270, RRID:AB_297008). All antibodies used were polyclonal and raised in rabbits, excluding those purchased from Santa Crux Biotechnology, which were raised in goats. Excess primary antibody was removed and successful binding was detected using rabbit anti-goat (Abcam, Cambridge, UK) or goat anti-rabbit (Thermo Fisher Scientific, Waltham, MA, USA) Alexa Fluor 488-conjugated secondary antibodies (1:1000 dilution). Finally, cells were mounted using VectaShield containing 1.5 µg/ml DAPI (Vector Laboratories, Peterborough, UK) and imaged using a Zeiss confocal microscope.

Immunohistochemistry

Fresh human subcutaneous adipose tissue was cut into 1 cm^2 pieces and washed with PBS to remove excess blood. Next, the tissue was submerged in 4% ice-cold PFA for four hours, then washed with PBS for 30 minutes twice and left in PBS overnight at 4°C. The tissue was then sequentially submerged in increasing concentrations of ethanol (30, 50, 70, 90, 95, 100% and 100%) for one hour each to dehydrate the tissue. The tissue was then submerged in histo-clear (National Diagnostic, Atlanta, GA, USA) for one hour and embedded into paraffin by placing the tissue in molten paraffin for two hours twice and the embedded tissue was placed in a mould and encased in paraffin. The paraffin embedded tissue was then left overnight at 4°C to set. The tissue was subsequently cut into 6 µm sections using a Microm HM355S automatic microtome (Thermo Fisher Scientific, Waltham, MA, USA) and mounted onto (3-aminopropyl)triethoxysilane coated glass slides. When the slides were dry, the sections were dewaxed with histo-clear (5 minutes twice) and rehydrated by sequentially submerging the sections in decreasing concentrations of ethanol (100, 95, 80, 70, 50 and 30% for 1 minute each), followed by distilled water for 1 minute. The dewaxed sections were then stained using an Anti-rabbit or Anti-goat HRP-DAB Cell & Tissue Staining Kit purchased from R and D systems (Minneapolis, MN, USA) as per the manufacturer's instructions. The sections were incubated with primary antibodies for $P2Y_1$ (Santa Cruz Biotechnology Cat# sc-20123, RRID:AB_2158393)), $P2Y_2$ (Santa Cruz Biotechnology Cat# sc-20124, RRID:AB_2156139)) or $P2Y_{12}$ (Santa Cruz Biotechnology Cat# sc-27152, RRID:AB_2155964) (1:200 in PBS with 1% BSA) or PBS with 1% BSA alone overnight at 4°C. All primary antibodies were purchased from Santa Cruz Biotechnology (Dallas, TX, USA). When the staining protocol was complete, the sections were dehydrated again by rapidly dipping the slides in increasing concentrations of ethanol, and then histo-clear for 10 minutes and finally mounted with DPX mountant. Once the mountant was dry, images of stained sections and no primary antibody controls were taken using an Olympus CKX41 inverted microscope (Olympus, Tokyo, Japan).

RNA extraction and cDNA synthesis

In vitro differentiated adipocytes were lysed with TRI-reagent and then treated with 100 µl 1-bromo-3-chloropropane and centrifuged to partition the sample. The top aqueous phase was then carefully transferred into a fresh tube and the RNA was precipitated with isopropanol and washed with 75% ethanol. The RNA was then centrifuged at 12,000 x *g* for 10 minutes, the supernatant was removed and the RNA pellet was air dried. The RNA was then resuspended in molecular grade water and potential genomic DNA contamination was removed using a

DNA-free™ DNA removal kit (Thermo Fisher Scientific, Waltham, MA, USA) as per the manufacturer's instructions. The purity and quantity of RNA was assessed using a Nanodrop 2000 (Thermo Scientific, Wilmington, DE, USA).

500 ng of RNA for each sample was primed with 100 ng random hexamer primers (Bioline, Taunton, MA, USA) by heating the mixture to 70°C for 10 minutes. Each sample was then incubated with 250 µM dNTPs (Bioline, Taunton, MA, USA), 30 U RNasin ribonuclease inhibitor (Promega, Madison, WI, USA), 0.01M DTT, first strand buffer and 200 U Superscript III Reverse transcriptase (RT) (Thermo Fisher Scientific, Waltham, MA, USA) for 1 hour at 42°C. A duplicate sample with no RT was run alongside as a control for genomic DNA contamination. The PCR reaction was terminated by heating the samples to 70°C for 10 minutes. Complementary DNA (cDNA) samples were then stored at -20°C.

Quantitative RT PCR

The cDNA and their corresponding no RT controls were diluted to 2 ng/µL and mixed with TaqMan™ fast universal PCR master mix (Thermo Fisher Scientific, Waltham, MA, USA). Commercially available TaqMan gene expression assay primers and probes for each gene of interest (GOI) were also added ($P2Y_1$ Hs00704965_s1; $P2Y_2$ Hs04176264_s1; $P2Y_4$ Hs00267404_s1; $P2Y_6$ Hs00366312_m1; $P2Y_{11}$ Hs01038858_m1; $P2Y_{12}$ Hs01881698_s1; $P2Y_{13}$ Hs03043902_s1; $P2Y_{14}$ Hs01848195_s1; P2X1 Hs00175686_m1; P2X2 Hs04176268_g1; P2X3 Hs01125554_m1; P2X4 Hs00602442_m1; P2X5 Hs01112471_m1; P2X6 Hs01003997_m1; P2X7 Hs00175721_m1; RPLP0 Hs99999902_m1). Each sample was then amplified in a MicroAmp fast optical 96-well reaction plate on an Applied Biosystems 7500 Real-Time PCR System (Thermo Fisher Scientific, Waltham, MA, USA) for 40 cycles. Threshold cycle (C_T) values were extracted from the 7500 software v2.0.6. Receptors with C_T values of below 35 were deemed to be expressed. Ribosomal protein lateral stalk subunit P0 (RPLP0) was used as an endogenous control to normalise for any variability in cDNA template input.

RT PCR

cDNA (or no RT control sample) (1 µg) was mixed with 25 µl of ReadyMix™ Taq PCR Reaction Mix, 0.2 µM forward primers, 0.2 µM reverse primers and water to achieve a total volume of 50 µl. The following PCR conditions were employed for each GOI: Initial denaturation at 94°C for 1 minute, then 35 cycles of 94°C for 30 seconds, variable annealing

conditions according to GOI and 72°C for 1 minute, followed by 5 minutes at 72°C for the final extension. The annealing conditions were 55°C for 30 seconds for all primer sequences, excluding adenylate cyclase type 2, 3, 8 and 9 that had an annealing temperature of 52°C (1 minute) and adenylate cyclase type 7, which had an annealing temperature of 45°C (1 minute). Primer sets used: adenylate cyclase type 1: sense 5' CAT GAC CTG CGA GGA CGA T 3', anti-sense 5' ACA GGA GAC TGC GAA TCT GAA 3'; type 2: sense 5' GGG GCT GCG TTT CTC T 3', anti-sense 5' CAG GAA CAC GGA ACA GGA TA 3'; type 3: sense 5' CAC GGG ACC CAG CAA T 3', anti-sense 5' GCT CTA AGG CCA CCA TAG GTA 3'; type 4: sense 5' TCC AAG CTC CCA ATG TGT CC 3', anti-sense 5' CTT GTC CAG AGG TGG CAT TT 3'; type 5: sense 5' TCT GGT CTA ACG ATG TCA CGC 3', anti-sense 5' TCT TTC CGC TTC TGG GTG C 3'; type 6: sense 5' GGC ATT GAT GAT TCC AGC AAA GAC 3', anti-sense 5' TGC AGG GCC TTA GGG AAC AGA 3'; type 7: sense 5' CCA GTC TGG ATG CAC AGG AG 3', anti-sense 5' AGC CTC CCA TCA AAG AAC CG 3'; type 8: sense 5' CGG GAT TTG GAA CGC CTC TA 3', anti-sense 5' CCG GTC TGA CAG GTA ACT GAT AA 3'; type 9: sense 5' CAC CGC AAA ATA CTT AGA TGA CG 3', anti-sense 5' CCT TCT CCT GCA AGA TCT CAC AC 3'.

Glycerol quantification assay

In vitro differentiated adipocytes were washed once with PBS and then incubated with 100 µl/well DMEM (without serum or antibiotics) for 2 hours at 37°C with 5% CO_2. Immediately following this incubation period, 1 µl/well vehicle or antagonist was added directly to each well and the cells were incubated for a further 30 minutes at 37°C with 5% CO_2. Next, a further 50 µl/well DMEM containing vehicle or agonists was added to each well. For the time series assays, a sample was collected immediately after the agonist was added by gently pipetting to mix and then 100 µl/well supernatant was removed and placed in a fresh 96 well plate and kept on ice for the duration of the experiment. These initial samples were labelled '0 minutes', and then samples were taken after 20, 40, 60, 120 and 180 minutes had lapsed. The cells were incubated at 37°C with 5% CO_2 between sample intervals. Alternatively, for all non-time series glycerol experiments, samples were taken three hours after vehicle/agonist was added. After the final sample was collected, all the samples were then stored at -80°C or used immediately for the glycerol quantification assay. A glycerol assay kit was purchased from Sigma Aldrich (Dorset, UK) and performed as per the manufacturer's instructions. A standard curve was run with each assay run. Due to variation in basal glycerol levels between donors, the data was normalised to the amount of glycerol produced under the control conditions after 3 hours.

ATP quantification assay

In vitro differentiated adipocytes were washed once with PBS and then incubated with 50 µl/well DMEM (without serum or antibiotics) for 1 hour at 37ºC with 5% CO_2. Next, 1 µl vehicle or antagonist was added directly to each well and the cells were incubated for a further 1 hour at 37ºC with 5% CO_2. The supernatant was then carefully removed, taking care not to disturb the cells, and the ATP was quantified using an ATP Bioluminescence Assay Kit HS II (Roche, Mannheim, Germany) performed as per the manufacturer's instructions. A standard curve was run with each assay. An integration time of 1 second was used for the bioluminescence readings. ATP levels in cell-free culture medium in each experimental condition were quantified and subtracted from test samples. The total cell number and supernatant volume were standardised for all experiments.

Cyclic AMP quantification assay

In vitro differentiated adipocytes were washed once with PBS and then incubated with 100 µl/well DMEM (no serum or antibiotics) for 2 hours at 37ºC and then the 1 µl/well vehicle/antagonist was added to each well and the cells were incubated for a further 30 minutes at 37ºC. DMEM alone or agonist (50 µl/well) was added to each well and the cells were incubated for a further 15 minutes at 37ºC. The cells were then washed twice with ice-cold PBS and lysed on ice with 100 µl/well 1x cell lysis buffer containing 1 mM phenylmethylsulfonyl fluoride. The rest of the assay was performed as per the manufacturer's instruction for the Cyclic AMP XP® Assay Kit (Cell Signalling Technology, Leiden, The Netherlands).

Lentiviral shRNA knockdown

Bacterial glycerol stocks of pLKO.1 puro vectors carrying Mission® non-target shRNA control sequences or shRNA sequences that targeted the $P2Y_2$ gene (TRCN0000009481) were purchased from Sigma-Aldrich (Dorset, UK). Bacterial stocks of psPAX2 (viral packaging plasmid) and pMD2.G (viral envelope plasmid) were purchased from Addgene (Cambridge, MA, USA). HEK239/17 cells (ATCC Cat# CRL-11268, RRID:CVCL 1926) were transfected with 12 µg psPAX2, 3 µg pMD2.G and 9 µg non-target shRNA control plasmid DNA (scrambled control) or plasmid DNA containing shRNA targeting $P2Y_2$ ($P2Y_2$ shRNA), in the presence of Lipofectamine™ 2000 (Thermo Fisher Scientific, Waltham, MA, USA). The HEK293/17 cells were grown in normal culture media (DMEM with 10% FBS and 1%

antibiotics) and this was exchanged for 20 ml of viral collection media (DMEM supplemented with 1% FBS and no antibiotics) immediately before adding the plasmid DNA and lipofectamine, which was diluted in 1.2 ml of OPTI-MEM media (Thermo Fisher Scientific, Waltham, MA, USA), drop-wise to the cells. The cells were then incubated for 6 hours with this mixture at 37°C in 5% CO_2. The media was then replaced with fresh viral collection media and then cells were left to incubate at 37°C in 5% CO_2 for 72 hours, with the media being collected (and stored at 4°C) and replaced with fresh viral collection media every 24 hours. After 72 hours had lapsed, the virus containing media was passed through a 0.45 um filter to remove cell debris and then the virus was concentrated using Lenti-X concentrator solution (Clontech, Fremont, CA, USA) as per the manufacturer's instructions. The resulting concentrated virus was then aliquoted and stored at -80°C until required. A p24 ELISA was performed using a QuickTiter™ Lentivirus Titer Kit (Cell Biolabs Inc, San Diego, CA, USA) as per the manufacturer's guidelines to calculate the multiplicity of infection (MOI) for both the scrambled control and $P2Y_2$ shRNA lentiviral particles. These values were then used to ensure that equivalent amounts of control and target lentivirus were used for subsequent experiments.

In vitro differentiated adipocytes were washed once with PBS and 200 µl/well of fresh culture media (DMEM containing 10% FBS and antibiotics) was added to each well. Then 8 µg/ml polybrene and scrambled control or $P2Y_2$ shRNA lentiviral particles (MOI of 1000) was added to each well and the cells were incubated for 18 hours at 37°C in 5% CO_2. The following day, the media was removed and replaced with fresh culture media and the cells were incubated for a further four days at 37°C in 5% CO_2 before they were ready for experimental use. Following experimental use, the cells were lysed and successful $P2Y_2$ knockdown was confirmed using quantitative RT PCR.

BODIPY staining

In vitro differentiated adipocytes transfected with scrambled control or $P2Y_2$ shRNA lentiviral particles were stained with BODIPY 493/503 lipid dye (Thermo Fisher Scientific, Waltham, MA, USA) to quantitate any changes in total lipid content due to reduction of $P2Y_2$ expression. To do this, the culture media was removed and replaced with 100 µl/well DMEM (no FBS or antibiotics) and a further 100 µl/well of DMEM containing 2 µM BODIPY 493/503 dye was added and immediately mixed thoroughly by gently pipetting. The cells were then incubated for 30 minutes at 37°C in the dark. The excess dye was then removed and the cells were washed

twice with PBS and then the fluorescence at 493/503 nm (excitation/emission) was measured using a Flexstation III microplate reader. Each experiment was normalised for background fluorescence, by measuring and subtracting the fluorescence values for cells in the absence of the dye.

Lipid droplet quantification

Images of human *in vitro* differentiated adipocytes that had been treated with both scrambled and $P2Y_2$ shRNA lentiviral particles were taken using an Olympus CKX41 inverted microscope for 12 independent donors. These images were then anonymised to eliminate operator bias and analysed using the counter plugin on Image J (NIH, Bethesda, MD, USA). The number of lipid droplets in 15 individual cells from each image were quantified. Once all the counting was complete, the values were sorted according to whether they were calculated from an image of scrambled or $P2Y_2$ knockdown adipocytes to perform statistical analyses.

Adipokine array

In vitro differentiated adipocytes were washed once with PBS and then incubated with 100 µl/well DMEM (no serum or antibiotics) for 2 hours at 37ºC in 5% CO_2. Next, 1 µl/well of vehicle or antagonist was added to each well and the cells were incubated for a further 30 minutes at 37ºC in 5% CO_2, then the first supernatant samples were taken for the 0 hour time point by gently pipetting up and down and then transferring 75 µl/well into a fresh 96 well plate. Additional samples were taken in this manner after 3 hours and 24 hours. All the samples were stored at -80ºC until required.

A Human Obesity Array Q3, which has the capacity to detect 40 human adipokine, was purchased from RayBiotech (Norcross, GA, USA). When supernatant samples had been collected from four independent donors, the samples were defrosted and allowed to warm to room temperature before conducting the protein array. The protein array was then performed as per the manufacturer's instruction and sent back to the manufacturer for analysis. The median fluorescence values were used for adipokine quantification analysis and a heat map was generated by normalising the average adipokine concentrations to the vehicle control.

Statistical analysis

Results were analysed, including statistical analyses, using Origin Pro 2017 software (Origin Lab, Northampton, MA, USA). All concentration response data were normalised to the maximal response. In cases of variability between donors, the concentration that produced the maximum response in the majority of donors was used. Data were normalised to their respective vehicle controls. Concentration response curves were fitted by Origin using the Hill Equation. *N* applies to number of donors throughout.

Data were assessed for normality using a Shapiro-Wilk test and then normally distributed data were assessed using a paired/unpaired Student's *t*-test or ANOVA with a post hoc Tukey test. Non-normally distributed data were assessed by paired sample Wilcoxon signed rank test, Mann-Whitney test or Kruskal-Wallis ANOVA with a post hoc Dunn's test. Data are expressed as mean ± SEM of experiments performed in duplicate using cells from a minimum of three independent donors.

Acknowledgements

This research is funded by the Biotechnology & Biological Sciences Research Council. We thank the support of the research nurses involved in the study at the Norfolk & Norwich University Hospital.

Author contributions

SA carried out all the experimental work. SA and SJF performed data analysis and experimental design. JT and SJF supervised the project. SJF wrote the manuscript.

References

Ahmadian, M., Wang, Y. & Sul, H.S., 2010. Lipolysis in adipocytes. *International Journal of Biochemistry and Cell Biology*, 42(5), pp.555–559. Available at: http://dx.doi.org/10.1016/j.biocel.2009.12.009.

Arruda, A.P. & Hotamisligil, G.S., 2015. Calcium Homeostasis and Organelle Function in the Pathogenesis of Obesity and Diabetes. *Cell metabolism*, 22(3), pp.381–97. Available at: http://www.ncbi.nlm.nih.gov/pubmed/26190652.

Ashour, F. & Deuchars, J., 2004. Electron microscopic localisation of P2X4 receptor subunit immunoreactivity to pre- and post-synaptic neuronal elements and glial processes in the dorsal vagal complex of the rat. *Brain Research*, 1026(1), pp.44–55. Available at: http://linkinghub.elsevier.com/retrieve/pii/S0006899304012855.

Bartness, T.J. et al., 2014. Neural innervation of white adipose tissue and the control of lipolysis. *Frontiers in neuroendocrinology*, 35(4), pp.473–93. Available at: http://www.ncbi.nlm.nih.gov/pubmed/24736043.

Bernstein, E.L. et al., 2004. Acute regulation of adiponectin by free fatty acids. *Metabolism: clinical and experimental*, 53(6), pp.790–3. Available at: http://www.ncbi.nlm.nih.gov/pubmed/15164330.

Bowers, R.R. et al., 2004. Sympathetic innervation of white adipose tissue and its regulation of fat cell number. *American journal of physiology. Regulatory, integrative and comparative physiology*, 286(6), pp.R1167-75. Available at: http://www.ncbi.nlm.nih.gov/pubmed/15142857.

Brand, C.S. et al., 2013. Isoform Selectivity of Adenylyl Cyclase Inhibitors: Characterization of Known and Novel Compounds. *Journal of Pharmacology and Experimental Therapeutics*, 347(2), pp.265–275.

Cioffi, D.L. et al., 2002. Dominant regulation of interendothelial cell gap formation by calcium-inhibited type 6 adenylyl cyclase. *The Journal of cell biology*, 157(7), pp.1267–78. Available at: http://www.ncbi.nlm.nih.gov/pubmed/12082084.

Clapham, D.E., 2007. Calcium Signaling. *Cell*, 131(6), pp.1047–1058. Available at: http://linkinghub.elsevier.com/retrieve/pii/S0092867407015310.

Corriden, R. & Insel, P.A., 2010. Basal release of ATP: an autocrine-paracrine mechanism

for cell regulation. *Science signaling*, 3(104), p.re1. Available at: http://www.ncbi.nlm.nih.gov/pubmed/20068232.

Gorini, S. et al., 2013. Regulation of innate immunity by extracellular nucleotides. *American Journal of Blood Research*, 3(1), pp.14–28.

Govindan, S. & Taylor, C.W., 2012. P2Y receptor subtypes evoke different Ca2+ signals in cultured aortic smooth muscle cells. *Purinergic Signalling*, 8(4), pp.763–777. Available at: http://link.springer.com/10.1007/s11302-012-9323-6.

Gray, N.E. et al., 2012. Angiopoietin-like 4 (Angptl4) protein is a physiological mediator of intracellular lipolysis in murine adipocytes. *The Journal of biological chemistry*, 287(11), pp.8444–56. Available at: http://www.ncbi.nlm.nih.gov/pubmed/22267746.

Greenberg, A.S. & Obin, M.S., 2006. Obesity and the role of adipose tissue in inflammation and metabolism. *The American journal of clinical nutrition*, 83(2), p.461S–465S. Available at: http://www.ncbi.nlm.nih.gov/pubmed/16470013.

Grynkiewicz, G., Poenie, M. & Tsien, R.Y., 1985. A new generation of Ca2+ indicators with greatly improved fluorescence properties. *The Journal of biological chemistry*, 260(6), pp.3440–50. Available at: http://www.ncbi.nlm.nih.gov/pubmed/3838314.

Halberg, N., Wernstedt, I. & Scherer, P.E., 2008. The Adipocyte as an Endocrine Cell. *Endocrinology and metabolism clinics of North America*, 37(3), p.753–xi. Available at: http://www.ncbi.nlm.nih.gov/pmc/articles/PMC2659415/.

Halls, M.L. & Cooper, D.M.F., 2011. Regulation by Ca2+-signaling pathways of adenylyl cyclases. *Cold Spring Harbor perspectives in biology*, 3(1), p.a004143. Available at: http://www.ncbi.nlm.nih.gov/pubmed/21123395.

Van Harmelen, V. et al., 1999. Mechanisms involved in the regulation of free fatty acid release from isolated human fat cells by acylation-stimulating protein and insulin. *The Journal of biological chemistry*, 274(26), pp.18243–51. Available at: http://www.ncbi.nlm.nih.gov/pubmed/10373426.

Heckmann, B.L. et al., 2014. Defective Adipose Lipolysis and Altered Global Energy Metabolism in Mice with Adipose Overexpression of the Lipolytic Inhibitor G 0 /G 1 Switch Gene 2 (G0S2). *Journal of Biological Chemistry*, 289(4), pp.1905–1916. Available at: http://www.jbc.org/lookup/doi/10.1074/jbc.M113.522011.

Hernandez-Olmos, V. et al., 2012. N-Substituted Phenoxazine and Acridone Derivatives: Structure–Activity Relationships of Potent P2X4 Receptor Antagonists. *Journal of Medicinal Chemistry*, 55(22), pp.9576–9588. Available at: http://pubs.acs.org/doi/abs/10.1021/jm300845v.

Hoffmann, K. et al., 2009. Interaction of New, Very Potent Non-Nucleotide Antagonists with Arg256 of the Human Platelet P2Y12 Receptor. *Journal of Pharmacology and Experimental Therapeutics*, 331(2), pp.648–655. Available at: http://jpet.aspetjournals.org/cgi/doi/10.1124/jpet.109.156687.

Jacobson, K.A. et al., 2009. Development of selective agonists and antagonists of P2Y receptors. *Purinergic Signalling*, 5(1), pp.75–89. Available at: http://link.springer.com/10.1007/s11302-008-9106-2.

Juan, C.-C. et al., 2005. Endothelin-1 induces lipolysis in 3T3-L1 adipocytes. *American journal of physiology. Endocrinology and metabolism*, 288(6), pp.E1146-52. Available at: http://www.ncbi.nlm.nih.gov/pubmed/15671081.

Jun, D.-J. et al., 2006. Sphingosine-1-phosphate modulates both lipolysis and leptin production in differentiated rat white adipocytes. *Endocrinology*, 147(12), pp.5835–44. Available at: http://www.ncbi.nlm.nih.gov/pubmed/16973728.

Katada, T., Tamura, M. & Ui, M., 1983. The A protomer of islet-activating protein, pertussis toxin, as an active peptide catalyzing ADP-ribosylation of a membrane protein. *Archives of biochemistry and biophysics*, 224(1), pp.290–8. Available at: http://www.ncbi.nlm.nih.gov/pubmed/6683482.

Kennedy, C., 2015. ATP as a cotransmitter in the autonomic nervous system. *Autonomic neuroscience : basic & clinical*, 191, pp.2–15. Available at: http://www.ncbi.nlm.nih.gov/pubmed/26054908.

Kim, H.S. et al., 2003. 2-Substitution of adenine nucleotide analogues containing a bicyclo[3.1.0]hexane ring system locked in a northern conformation: enhanced potency as P2Y1 receptor antagonists. *Journal of medicinal chemistry*, 46(23), pp.4974–87. Available at: http://www.ncbi.nlm.nih.gov/pubmed/14584948.

Kim, Y.-C. et al., 2005. Synthesis of pyridoxal phosphate derivatives with antagonist activity at the P2Y13 receptor. *Biochemical Pharmacology*, 70(2), pp.266–274. Available at: http://linkinghub.elsevier.com/retrieve/pii/S0006295205002558.

Kotnis, S. et al., 2010. Genetic and Functional Analysis of Human P2X5 Reveals a Distinct Pattern of Exon 10 Polymorphism with Predominant Expression of the Nonfunctional Receptor Isoform. *Molecular Pharmacology*, 77(6), pp.953–960. Available at: http://molpharm.aspetjournals.org/cgi/doi/10.1124/mol.110.063636.

Krzyzanowska, K. et al., 2007. Adiponectin concentrations increase during acute FFA elevation in humans treated with rosiglitazone. *Hormone and metabolic research = Hormon- und Stoffwechselforschung = Hormones et metabolisme*, 39(10), pp.769–72.

Available at: http://www.ncbi.nlm.nih.gov/pubmed/17952842.

von Kügelgen, I. & Hoffmann, K., 2016. Pharmacology and structure of P2Y receptors. *Neuropharmacology*, 104, pp.50–61. Available at: http://linkinghub.elsevier.com/retrieve/pii/S0028390815301532.

Lazarowski, E.R. et al., 1995. Pharmacological selectivity of the cloned human P2U-purinoceptor: potent activation by diadenosine tetraphosphate. *British Journal of Pharmacology*, 116(1), pp.1619–1627. Available at: http://doi.wiley.com/10.1111/j.1476-5381.1995.tb16382.x.

Lee, S.-A. et al., 2016. Adipocyte-specific overexpression of retinol-binding protein 4 causes hepatic steatosis in mice. *Hepatology (Baltimore, Md.)*, 64(5), pp.1534–1546. Available at: http://www.ncbi.nlm.nih.gov/pubmed/27227735.

Mamedova, L.K. et al., 2004. Diisothiocyanate derivatives as potent, insurmountable antagonists of P2Y6 nucleotide receptors. *Biochemical Pharmacology*, 67(9), pp.1763–1770. Available at: http://linkinghub.elsevier.com/retrieve/pii/S0006295204000620.

Meis, S. et al., 2010. NF546 [4,4'-(Carbonylbis(imino-3,1-phenylene-carbonylimino-3,1-(4-methyl-phenylene)-carbonylimino))-bis(1,3-xylene- , '-diphosphonic Acid) Tetrasodium Salt] Is a Non-Nucleotide P2Y11 Agonist and Stimulates Release of Interleukin-8 from Human Monocyte-Deri. *Journal of Pharmacology and Experimental Therapeutics*, 332(1), pp.238–247. Available at: http://jpet.aspetjournals.org/cgi/doi/10.1124/jpet.109.157750.

Micklewright, J.J., Layhadi, J.A. & Fountain, S.J., 2018. P2Y 12 receptor modulation of ADP-evoked intracellular Ca 2+ signalling in THP-1 human monocytic cells. *British Journal of Pharmacology*, 175(12), pp.2483–2491. Available at: http://doi.wiley.com/10.1111/bph.14218.

Miyoshi, H. et al., 2008. Adipose triglyceride lipase regulates basal lipolysis and lipid droplet size in adipocytes. *Journal of cellular biochemistry*, 105(6), pp.1430–6. Available at: http://www.ncbi.nlm.nih.gov/pubmed/18980248.

Miyoshi, H. et al., 2006. Perilipin promotes hormone-sensitive lipase-mediated adipocyte lipolysis via phosphorylation-dependent and -independent mechanisms. *The Journal of biological chemistry*, 281(23), pp.15837–44. Available at: http://www.ncbi.nlm.nih.gov/pubmed/16595669.

Nelson, D.W. et al., 2006. Structure−Activity Relationship Studies on a Series of Novel, Substituted 1-Benzyl-5-phenyltetrazole P2X 7 Antagonists. *Journal of Medicinal Chemistry*, 49(12), pp.3659–3666. Available at:

http://pubs.acs.org/doi/abs/10.1021/jm051202e.

Nielsen, T.S. et al., 2014. Dissecting adipose tissue lipolysis: molecular regulation and implications for metabolic disease. *Journal of Molecular Endocrinology*, 52(3), pp.R199–R222. Available at: http://jme.endocrinology-journals.org/cgi/doi/10.1530/JME-13-0277.

North, R. a, 2002. Molecular physiology of P2X receptors. *Physiological reviews*, 82(4), p.1013–67. Available at: http://www.google.com/search?client=safari&rls=en-us&q=Molecular+physiology+of+P2X+receptors&ie=UTF-8&oe=UTF-8%5Cnpapers2://publication/uuid/ECEB72C8-E566-4DEC-8229-186B97F833BE.

Omori, K. & Kotera, J., 2007. Overview of PDEs and their regulation. *Circulation research*, 100(3), pp.309–27. Available at: http://www.ncbi.nlm.nih.gov/pubmed/17307970.

Ormond, S.J., 2006. An Uncharged Region within the N Terminus of the P2X6 Receptor Inhibits Its Assembly and Exit from the Endoplasmic Reticulum. *Molecular Pharmacology*, 69(5), pp.1692–1700. Available at: http://molpharm.aspetjournals.org/cgi/doi/10.1124/mol.105.020404.

La Paglia, L. et al., 2017. Potential Role of ANGPTL4 in the Cross Talk between Metabolism and Cancer through PPAR Signaling Pathway. *PPAR Research*, 2017, pp.1–15. Available at: https://www.hindawi.com/journals/ppar/2017/8187235/.

Qiao, L. et al., 2011. Energy intake and adiponectin gene expression. *American journal of physiology. Endocrinology and metabolism*, 300(5), pp.E809-16. Available at: http://www.ncbi.nlm.nih.gov/pubmed/21325106.

Rafehi, M. et al., 2017. Synthesis, characterization, and in vitro evaluation of the selective P2Y2 receptor antagonist AR-C118925. *Purinergic Signalling*, 13(1), pp.89–103. Available at: http://link.springer.com/10.1007/s11302-016-9542-3.

Ronti, T., Lupattelli, G. & Mannarino, E., 2006. The endocrine function of adipose tissue: an update. *Clinical endocrinology*, 64(4), pp.355–65. Available at: http://www.ncbi.nlm.nih.gov/pubmed/16584505.

Rosen, E.D. & Spiegelman, B.M., 2006. Adipocytes as regulators of energy balance and glucose homeostasis. *Nature*, 444(7121), pp.847–853.

Rutkowski, J.M., Stern, J.H. & Scherer, P.E., 2015. The cell biology of fat expansion. *The Journal of Cell Biology*, 208(5), pp.501–512. Available at: http://www.jcb.org/lookup/doi/10.1083/jcb.201409063.

Rydén, M. & Arner, P., 2017. Subcutaneous Adipocyte Lipolysis Contributes to Circulating Lipid Levels. *Arteriosclerosis, Thrombosis, and Vascular Biology*, 37(9), pp.1782–1787.

Available at: http://atvb.ahajournals.org/lookup/doi/10.1161/ATVBAHA.117.309759.

Shi, H. et al., 2000. Role of intracellular calcium in human adipocyte differentiation. *Physiological genomics*, 3(2), pp.75–82. Available at: http://www.ncbi.nlm.nih.gov/pubmed/11015602.

Sivaramakrishnan, V. et al., 2012. Constitutive lysosome exocytosis releases ATP and engages P2Y receptors in human monocytes. *Journal of cell science*, 125(Pt 19), pp.4567–75. Available at: http://www.ncbi.nlm.nih.gov/pubmed/22767503.

Snyder, P.B. et al., 2005. The role of cyclic nucleotide phosphodiesterases in the regulation of adipocyte lipolysis. *Journal of Lipid Research*, 46(3), pp.494–503. Available at: http://www.jlr.org/lookup/doi/10.1194/jlr.M400362-JLR200.

Stokes, L., 2013. Rab5 regulates internalisation of P2X4 receptors and potentiation by ivermectin. *Purinergic Signalling*, 9(1), pp.113–121. Available at: http://link.springer.com/10.1007/s11302-012-9336-1.

Sukumar, P. et al., 2012. Constitutively active TRPC channels of adipocytes confer a mechanism for sensing dietary fatty acids and regulating adiponectin. *Circulation research*, 111(2), pp.191–200. Available at: http://www.ncbi.nlm.nih.gov/pubmed/22668831.

Torres, G.E., Egan, T.M. & Voigt, M.M., 1999. Hetero-oligomeric Assembly of P2X Receptor Subunits. *Journal of Biological Chemistry*, 274(10), pp.6653–6659. Available at: http://www.jbc.org/lookup/doi/10.1074/jbc.274.10.6653.

Turner, J.J.O. et al., 2010. Investigation of nuclear factor-κB inhibitors and interleukin-10 as regulators of inflammatory signalling in human adipocytes. *Clinical & Experimental Immunology*, 162(3), pp.487–493. Available at: http://doi.wiley.com/10.1111/j.1365-2249.2010.04260.x.

Wang, H. et al., 2011. Unique regulation of adipose triglyceride lipase (ATGL) by perilipin 5, a lipid droplet-associated protein. *The Journal of biological chemistry*, 286(18), pp.15707–15. Available at: http://www.ncbi.nlm.nih.gov/pubmed/21393244.

Wedellová, Z. et al., 2011. Adiponectin inhibits spontaneous and catecholamine-induced lipolysis in human adipocytes of non-obese subjects through AMPK-dependent mechanisms. *Physiological research*, 60(1), pp.139–48. Available at: http://www.ncbi.nlm.nih.gov/pubmed/20945960.

Weisberg, S.P. et al., 2003. Obesity is associated with macrophage accumulation in adipose tissue. *Journal of Clinical Investigation*, 112(12), pp.1796–1808. Available at: http://www.jci.org/articles/view/19246.

Xue, B. et al., 2001. Mechanism of intracellular calcium ([Ca2+]i) inhibition of lipolysis in human adipocytes. *FASEB journal : official publication of the Federation of American Societies for Experimental Biology*, 15(13), pp.2527–9. Available at: http://www.ncbi.nlm.nih.gov/pubmed/11641262.

Yegutkin, G.G., 2008. Nucleotide- and nucleoside-converting ectoenzymes: Important modulators of purinergic signalling cascade. *Biochimica et biophysica acta*, 1783(5), pp.673–94. Available at: http://www.sciencedirect.com/science/article/pii/S0167488908000396 [Accessed April 15, 2015].

Zhang, H.H. et al., 2002. Tumor necrosis factor-alpha stimulates lipolysis in differentiated human adipocytes through activation of extracellular signal-related kinase and elevation of intracellular cAMP. *Diabetes*, 51(10), pp.2929–35. Available at: http://www.ncbi.nlm.nih.gov/pubmed/12351429.

Figures

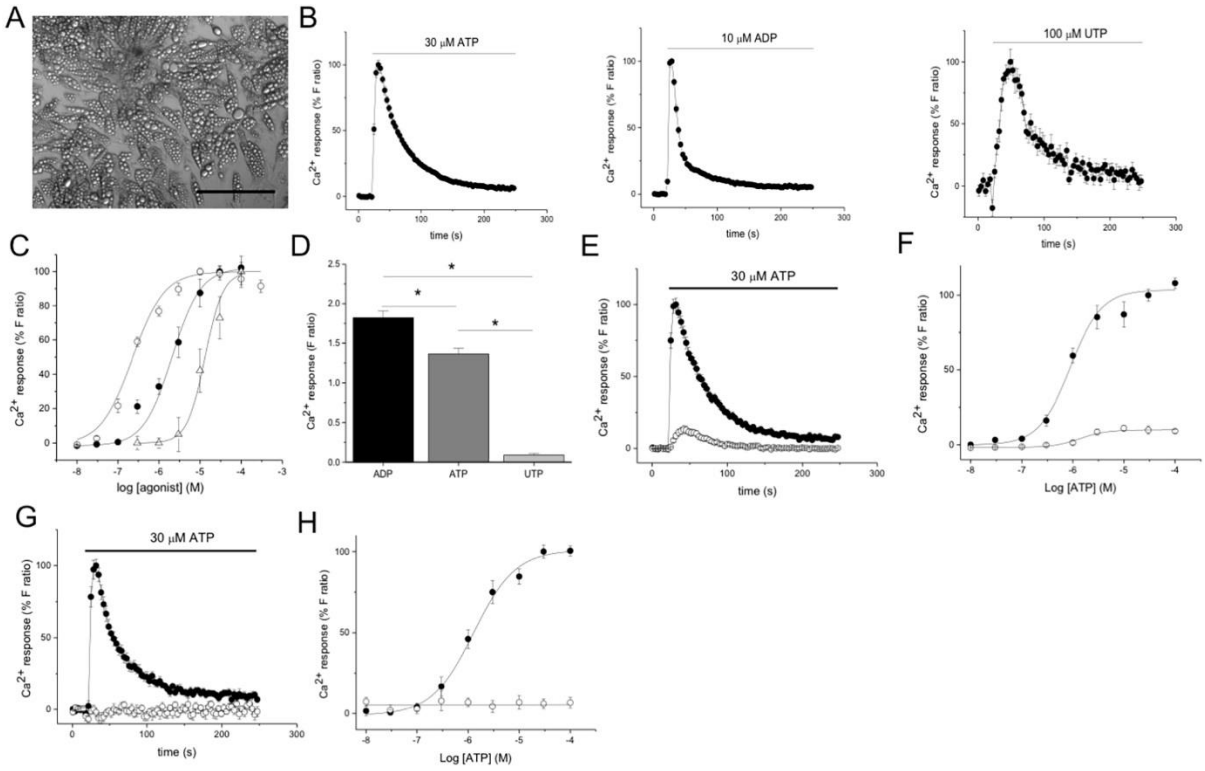

Figure 1 Extracellular ATP, ADP and UTP elicited intracellular Ca^{2+} responses in human adipocytes. (A) Representative image of human adipocytes in culture. Scale bar represents 100μm. (B) Time-resolved intracellular Ca^{2+} responses for maximal concentrations of ATP, ADP and UTP (*N*=6). Traces are normalized to peak response. (C) Concentration response relationship for Ca^{2+} responses evoked by ATP (*closed circles*), ADP (*open circles*) and UTP (*open triangles*) (*N*=6). (D) Chart to show significant differences in Ca^{2+} response maxima evoked by nucleotides at maximal concentrations (ATP, 30μM; ADP, 10μM; UTP, 100μM) (*N*=6; **P*<0.05). (E) Time resolved intracellular Ca^{2+} response evoked by ATP in the presence (*closed circles*) and absence (*open circles*) of extracellular Ca^{2+} (*N*=6). (F) ATP concentration-response curve in the presence (*closed circles*) and absence (*open circles*) of extracellular Ca^{2+} (*N*=6). (G) Effect of phospholipase C inhibition on intracellular Ca^{2+} responses evoked by ATP. Ca^{2+} signal evoked by ATP in the presence (*open circles*) and absence (*closed circles*) of 10μM U73122 (*N*=6). (H) Concentration-response curve for ATP in the presence (*open circles*) and absence (*closed circles*) of 10μM U73122 (*N*=6). *F* ratio represents the emission ratio of Fura-2 throughout. *N* represents number of donors (biological repeats).

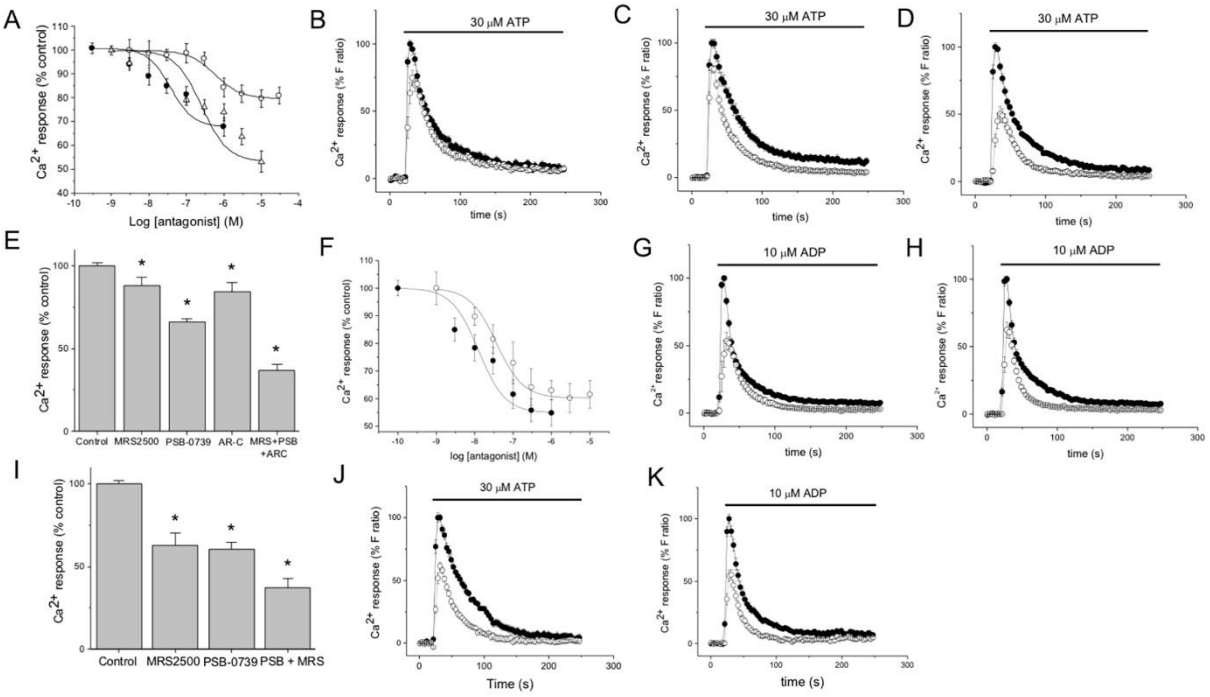

Figure 2 $P2Y_1$, $P2Y_2$ and $P2Y_{12}$ receptor activation mediates ATP-evoked Ca^{2+} signaling and $P2Y_1$ and $P2Y_{12}$ receptor activation mediates ADP-evoked Ca^{2+} signaling in human adipocytes. (**A**) Effect of P2Y subtype selective antagonists on Ca^{2+} responses evoked by 30μM ATP. Concentration-inhibition curve for MRS2500 ($P2Y_1$; *closed circles*), AR-C118925XX ($P2Y_2$; *open circles*) and PSB0739 ($P2Y_{12}$; *triangles*) (*N*=6). Responses are normalized to the agonist response in the presence of vehicle control only. (**B-D**) Time resolved Ca^{2+} response evoked by ATP in the presence (*open circles*) and absence (*closed circles*) of 1μM MRS2500 (**B**), 10μM AR-C118925XX (**C**) or 10μM PSB-0739 (**D**) (*N*=6). Traces are normalized to peak agonist response in the presence of vehicle control only. (**E**) Chart to show effects of individual antagonists (MRS2500, 1μM; AR-C118925XX, 10 μM; PSB-0739, 3μM), or in combination, on the magnitude of Ca^{2+} response evoked by 30μM ATP (*N*=6; **P*<0.05 versus vehicle control). (**F**) Effect of $P2Y_1$ and $P2Y_{12}$ receptor antagonists subtype selective inhibitors on Ca^{2+} responses evoked by 10μM ADP. Concentration-inhibition curve for MRS2500 ($P2Y_1$; *closed circles*) and PSB-0739 ($P2Y_{12}$; *open circles*) (*N*=6). (**G** and **H**) Time resolved Ca^{2+} response evoked by ADP in the presence (*open circles*) and absence (*closed circles*) of 1μM MRS2500 (**G**), 3μM PSB-0739 (**H**) or 10μM AR-C118925XX (*N*=6). (**I**) Chart to show effects of individual antagonists (MRS2500, 1μM; PSB-0739, 3μM), or in combination, on the magnitude of Ca^{2+} response evoked by 10μM ADP (*N*=6; **P*<0.05 versus

vehicle control). (**J**) Effect of 100 ng/mL pertussis on Ca^{2+} responses evoked by ATP (**J**) or ADP (**K**). Traces shown are for vehicle control (*closed circles*) or with pertussis toxin (*open circles*). *F* ratio represents the emission ratio of Fura-2 throughout. *N* represents number of donors (biological repeats).

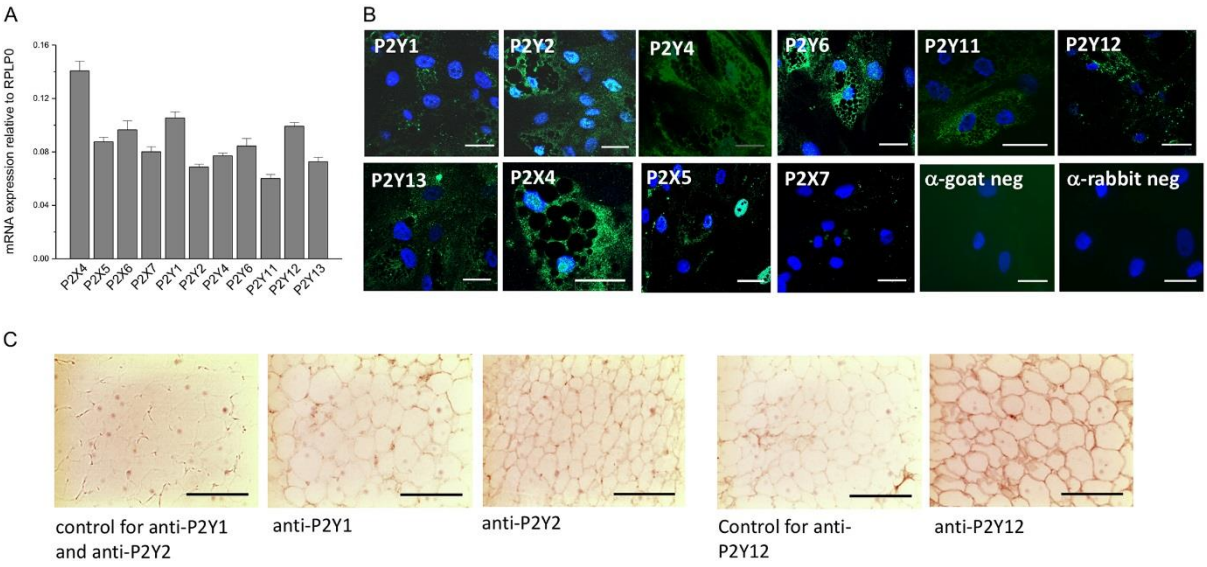

Figure 3 Expression of purinergic receptors in human adipocytes and adipose tissue. (**A**) Quantitative RT-PCR analysis of P2Y and P2X receptor subtypes expressed by adipocytes (*N*=6 donors). Expression is given relative to the housekeeper gene, RPLP0. (**B**) Immunocytochemical staining of purinergic receptor subtypes in human adipocytes. Rabbit polyclonal primary antibodies against $P2X_4$, $P2X_7$, $P2Y_1$, $P2Y_2$, $P2Y_4$, $P2Y_6$, $P2Y_{11}$, $P2Y_{13}$ receptors, and goat polyclonal primary antibodies against $P2X_5$ and $P2Y_{12}$ receptors are used. Green channel shows fluorescence arising from secondary anti-rabbit or anti-goat Alexa 488-conjugated antibodies. (α-goat neg or α-rabbit neg) Non-specific binding negative controls for secondary antibodies. Blue channel shows nuclei counterstained with DAPI. Scale bar is 30µm. Images are representative of at least 10 fields of view for 3 donors. (**C**) anti-$P2Y_1$, anti-$P2Y_2$ and anti-$P2Y_{12}$ immunoreactivity in 6µm sections of human abdominal subcutaneous white adipose tissue. Immunoreactivity visualized using a HRP-conjugated secondary antibody. Non-specific secondary binding controlled for in the absence of anti-P2Y receptor antibody (*no primary controls*). Scale bar is 200µm.

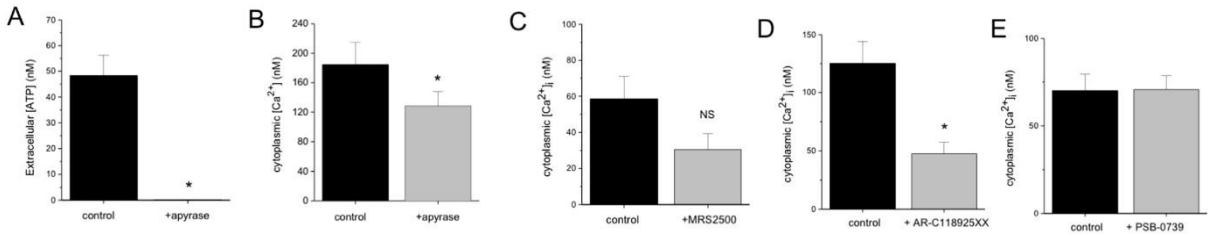

Figure 4 Adipocyte cytoplasmic Ca^{2+} tone generated by constitutive ATP release and $P2Y_2$ receptor activation. (**A**) Luciferase bioluminescence measurement of extracellular ATP in culture medium conditioned by human adipocytes under control conditions and following extracellular ATP scavenging with apyrase (4U/mL) (*N*=3). (**B**) Resting cytoplasmic Ca^{2+} in adipocytes in control conditions or following treatment with apyrase (4U/ml) for 30 minutes (*N*=4). (**C-E**) Effect of P2Y receptor subtype antagonists on adipocyte resting cytoplasmic Ca^{2+}. Cells treated with MRS2500 (**C**; 1µM; $P2Y_1$), AR-C118925XX (**D**; 10 µM; $P2Y_2$) or PSB-0739 (**E**; 1µM; $P2Y_{12}$) for 30 minutes or vehicle (control) (*N*=6). Ca^{2+} concentrations are calculated via the calibration of the ratiometric Ca^{2+} indicator Fura-2. **P*<0.05 versus control throughout; *NS* is non-significant; *N* represents number of donors (biological repeats).

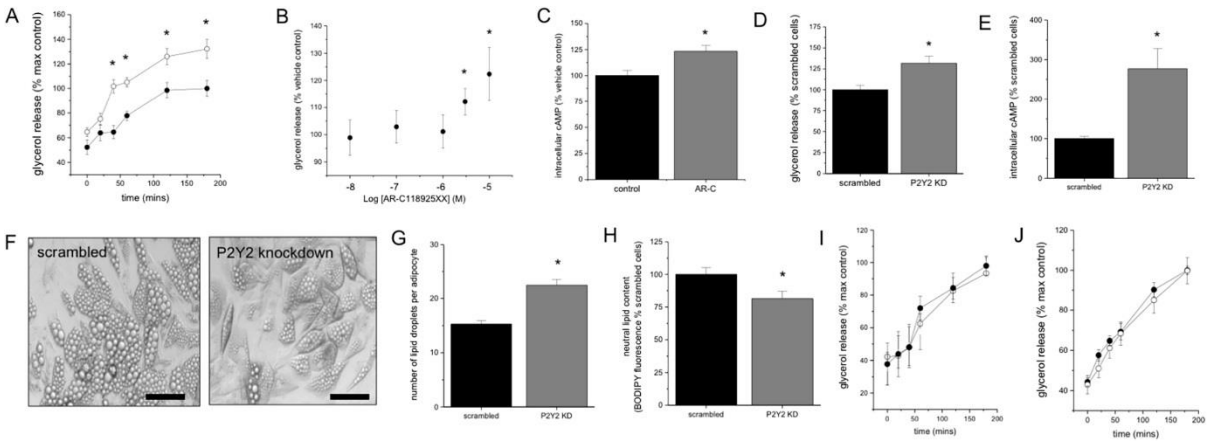

Figure 5 $P2Y_2$ receptor antagonism or knockdown enhances basal lipolysis in human adipocytes. (**A**) Basal lipolysis measured in adipocytes in culture by glycerol release. Adipocytes are in the presence of vehicle (*closed circles*) or with $P2Y_2$ antagonist (AR-C118925XX, 10 µM; *open circles*) (*N*=3). (**B**) Concentration dependent enhancement of basal lipolysis by AR-C118925XX. Data is shown is for glycerol release after 3 hours as a percentage of vehicle control (*N*=3). (**C**) Change in intracellular cyclic AMP in response to $P2Y_2$ antagonism (AR-C118925XX, 10 µM; 45 mins) over vehicle control (*N*=4). (**D**) Change in basal lipolysis following shRNA-mediated $P2Y_2$ receptor knockdown in adipocytes versus scrambled counterparts (*N*=3). Glycerol release measured for 3 hours. (**E**) Change in intracellular cyclic AMP in $P2Y_2$ receptor knockdown adipocytes versus scrambled counterparts (*N*=3). (**F**) Representative (*N*=12) brightfield images to illustrate the small lipid droplet phenotype observed in $P2Y_2$ receptor knockdown adipocytes versus scrambled counterparts. Scale bar is 50µm. (**G** and **H**) Quantitation of number of lipid droplets (**G**; *N*=12) and neutral lipid content (**H**; BODIPY fluorescence; *N*=6) in $P2Y_2$ receptor knockdown adipocyte versus scrambled counterparts. (**I** and **J**) Lack of effect of $P2Y_1$ receptor (**I**; MRS2500, 1µM; *open circles; N*=3) or $P2Y_{12}$ receptor (**J**; PSB-0739, 3µM; *open circles; N*=5) antagonism on basal lipolysis. **P*<0.05 versus control throughout; *NS* is non-significant; *N* represents number of donors (biological repeats).

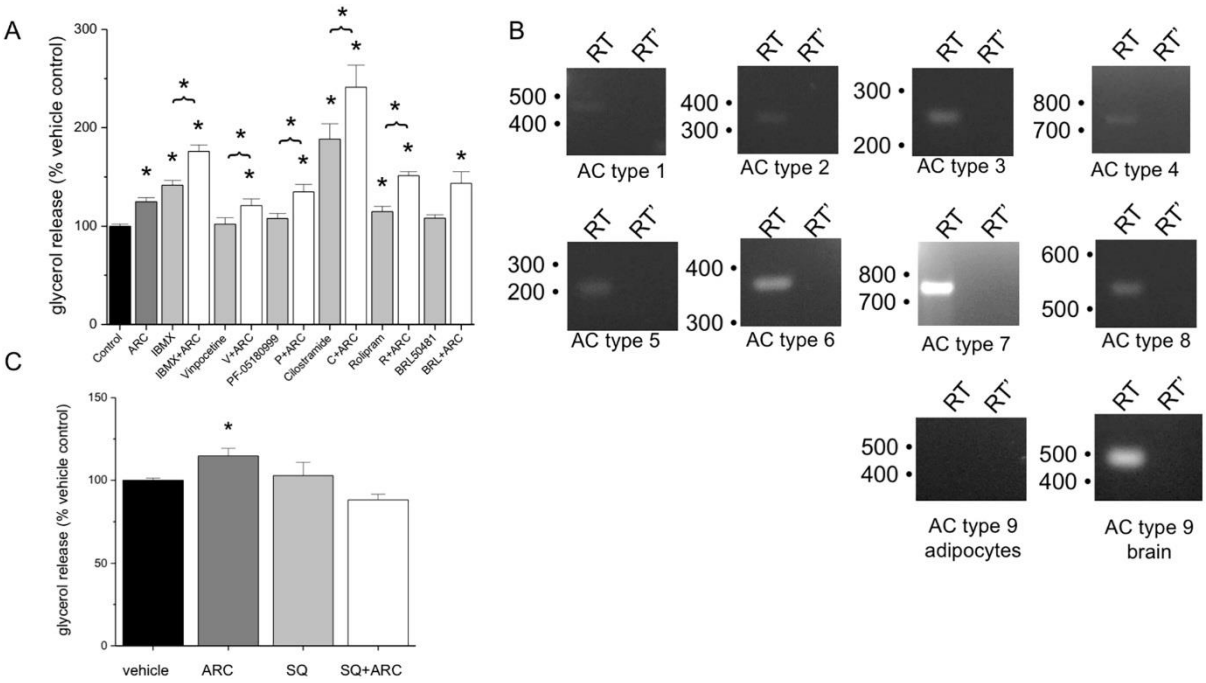

Figure 6 P2Y$_2$ receptor antagonism synergises with phosphodiesterase inhibition, but is dependent on adenylate cyclase activity in enhancing basal lipolysis in human adipocytes

(A) Effect of antagonising phosphodiesterase (PDE) isoforms on basal lipolysis with and without P2Y$_2$ antagonism. P2Y$_2$ (AR-C118925XX, 10 μM), IBMX (pan PDE inhibitor; 10μM), vinpocetine (PDE1; 10μM), PF-05180999 (PDE2; 10μM), cilostamide (PDE3; 1μM), rolipram (PDE4; 10μM) and BRL50481 (PDE7; 1μM) (*N*=3). Glycerol release after 3 hours expressed as percentage vehicle control. (**B**) RT-PCR detection of adenylate cyclase isoforms in human adipocytes. Expected product sizes AC type 1 (446 bp), type 2 (369 bp), type 3 (263 bp), type 4 (753 bp), type 5 (202 bp), type 6 (380 bp), type 7 (746 bp), type 8 (543 bp) and type 9 (497 bp). *Brain* denotes positive control for AC type 9 expression. RT' denotes absence of reverse transcriptase (negative control for genomic DNA). (**C**) Effect of P2Y$_2$ receptor antagonism (AR-C118925XX, 10 μM) on basal lipolysis is reversed following adenylate cyclase inhibition (SQ22536, 1μM) (*N*=6). Basal lipolysis is measured as glycerol release over 3 hours in all experiments. Antagonists were added 30 minutes prior to the start of the assay. **P*<0.05 versus control throughout; *N* represents number of donors (biological repeats).

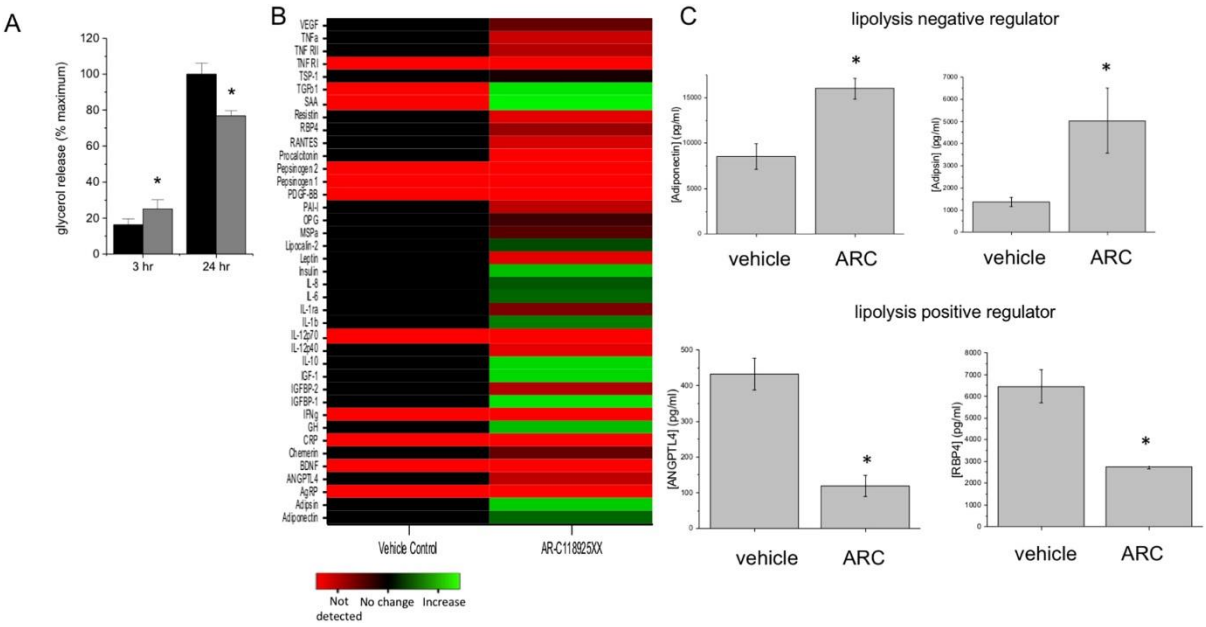

Figure 7 Longer term suppression of basal lipolysis in human adipocytes following P2Y$_2$ receptor antagonism is associated with an anti-lipolytic adipokine profile. (**A**) Glycerol release (basal lipolysis) measured 3 hours and 24 hours after singular exposure to vehicle (*black bars*) or P2Y$_2$ antagonist (AR-C118925XX, 10μM; *grey bars*) (*N*=4). (**B**) Heat map representing average change in secreted adipokines 24 hours after adipocyte exposure to vehicle or 10μM AR-C118925XX (*N*=4), as determined by quantitative protein array. Fold changes are expressed relative to levels of secreted adipokines before exposure to vehicle or AR-C118925XX. Bar charts showing significant increases in adiponectin and adipsin (negative regulators of lipolysis), and decrease in ANGPTL4 and RBP (positive regulators of lipolysis to illustrate shift to anti-lipolytic adipokine profile 24 hours after adipocyte singular exposure to 10μM AR-C118925XX (*N*=4). **P*<0.05 versus control. *N* represents number of donors (biological repeats).

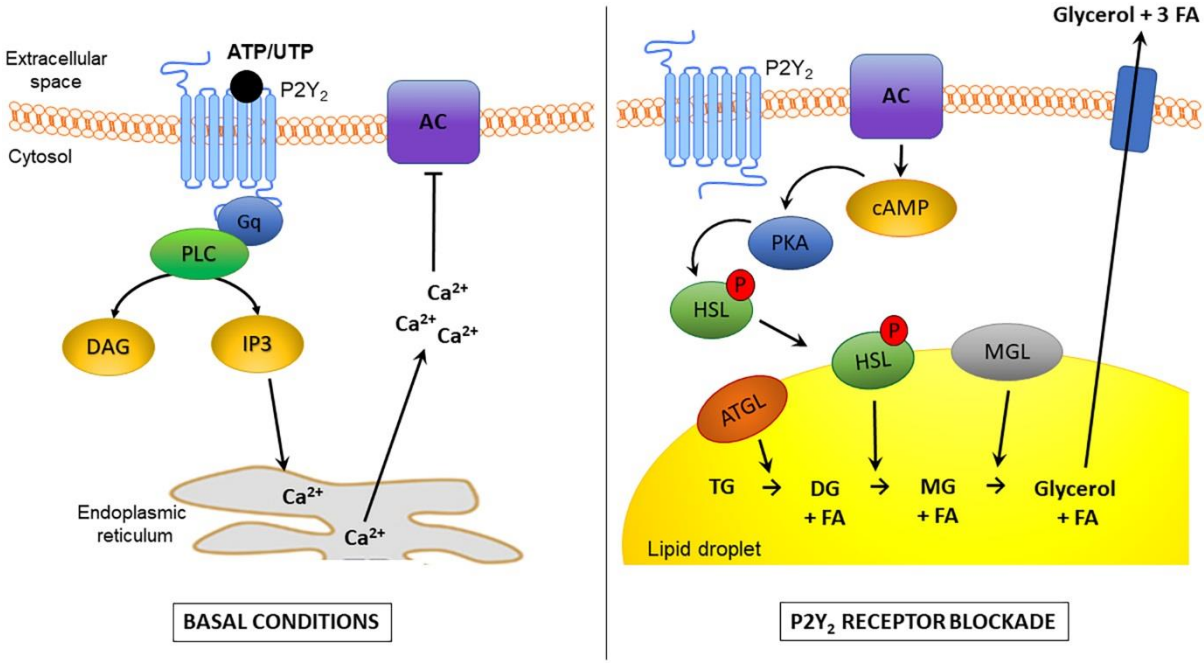

Figure 8 Schematic diagram of the proposed mechanism by which P2Y$_2$ receptor activation causes acute suppression of lipolysis in primary human *in vitro* differentiated adipocytes. Under basal conditions (left hand panel), P2Y$_2$ receptors are activated by ATP or UTP released by the adipocytes into the extracellular space, which then subsequently activates phospholipase C (PLC) mediated production of diacylglycerol (DAG) and inositol triphosphate (IP3). The IP3 then binds to receptors on the surface of the endoplasmic reticulum (ER) to initiate release of calcium ions (Ca^{2+}) from the ER into the cytosol. This elevation of cytoplasmic calcium causes tonic inhibition of calcium-sensitive adenylate cyclase (AC) isoforms. However, in the absence of P2Y$_2$-receptor mediated inhibition of AC due to blockade of P2Y$_2$ receptor signalling (right hand panel), intracellular calcium concentrations are lower and therefore AC is not inhibited and consequently free to convert ATP to cyclic AMP (cAMP). The increase in intracellular cAMP activates protein kinase A (PKA), which is then able to phosphorylate cytoplasmic hormone sensitive lipase (HSL). This allows HSL to translocate the lipid droplet. Here, adipose triglyceride lipase (ATGL) catalyses the hydrolysis of triglycerides (TG) to diglycerides (DG) and a free fatty acid (FA) molecule, then HSL catalyses the conversion of DG to monoglycerides (MG) and FA, finally monoglyceride lipase (MGL) catalyses lipolytic breakdown of MG to glycerol and FA. The glycerol and three FA molecules can then be transported out of the cell and released into the bloodstream, where they can travel to the liver or other organs to be utilised as an energy source

Supplementary Table 1 The effect of P2 subtype selective antagonism on the nucleotide-evoked calcium responses in primary human *in vitro* differentiated adipocytes. All the values in the maximum inhibition and IC_{50} columns were determined using cells from 6 independent donors.

Selective antagonist	Receptor target	Nucleotide [concentration, µM]	Antagonist range, µM	Maximum inhibition (%)[a] [antagonist concentration, µM]	IC_{50}, nM[a]	Reference
PSB-12062	P2X4	ATP [100]	0.003 – 30	*NS*	-	(Hernandez-Olmos et al. 2012)
A438079	P2X7	ATP [1000]	0.003 – 10	*NS*	-	(Nelson et al. 2006)
MRS2500	$P2Y_1$	ATP [30]	0.0001 – 1	32.3 ± 3.8 [1]	415 ± 160	(Kim et al. 2003)
				33.6 ± 3.6 [1]	>1000	
		ADP [10]	0.0001 – 1	45.1 ± 4.7 [1]	77.1 ± 37.5	
				45.4 ± 6.9 [1]	>1000	
AR-C118925XX	$P2Y_2$	ATP [30]	0.003 - 30	20.4 ± 3.6 [10]	683 ± 116	(Rafehi et al. 2017)
				47 ± 1.7 [10]	434 ± 133	
		UTP [30]	0.003 - 30	100%	318 ± 399	
				100%	474 ± 527	
MRS2578	$P2Y_6$	ADP [30]	0.003 – 10	*NS*	-	(Mamedova et al. 2004)
NF340	$P2Y_{11}$	ATP [30]	0.003 - 10	*NS*	-	(Meis et al. 2010)
		ADP [10]	0.003 – 10	*NS*	-	
PSB-0739	$P2Y_{12}$	ATP [30]	0.003 – 10	46.8 ± 4.5 [10]	<10,000	(Hoffmann et al. 2009)
				44.5 ± 5.2 [10]	<10,000	
		ADP [10]	0.003 – 10	38.4 ± 5.1 [10]	64.0 ± 56.5	
				55.4 ± 4.4 [10]	162 ± 25.4	
MRS2211	$P2Y_{13}$	ATP [30]	0.003 – 3	*NS*	-	(Kim et al. 2005)
		ADP [10]	0.003 – 3	*NS*	-	

[a]IC_{50} values and max % inhibition values were calculated with the peak magnitude values (top) and area under the curve data (bottom) for each agonist/antagonist combination. *NS* indicates no significant inhibition at any concentration of antagonist tested.

Supplementary Table 2 The adipokine profile secreted by primary human *in vitro* differentiated adipocytes following singular treatment with vehicle or $P2Y_2$ receptor antagonist (AR-C118925XX). Adipokines are quantified by protein array and data are presented as mean ± s.e.m for four donors.

	Vehicle control (pg/ml)	10 µM AR-C118925XX (pg/ml)	% increase or decrease	Significance (p value)
Adiponectin	8542.1 ± 1404	16001.1 ± 1156	↑ 87%	0.000009
Adipsin	1360.5 ± 208	5024.4 ± 1468	↑ 269%	0.0005
AgRP	<14	<14	-	-
ANGPTL4	432.4 ± 45	119.7 ± 30	↓ 72%	0.0007
BDNF	<55	<55	-	-
Chemerin	602.1 ± 140	374.6 ± 70	-	0.4
CRP	<27	12.6 ± 4	-	0.04
GH	<27	45.1 ± 11	↑ 100%	0.03
IFNγ	<14	<14	-	-
IGFBP-1	15.3 ± 5	346.8 ± 28	↑ 2162%	0.0005
IGFBP-2	756.4 ± 57	262.9 ± 20	↓ 65%	0.0000001
IGF-1	4921.0 ± 1077	41515.3 ± 2087	↑ 744%	0.0000000009
IL-10	1.8 ± 0.5	8.5 ± 2	↑ 369%	0.004
IL-12p40	220.2 ± 95	32.2 ± 9	-	0.3
IL-12p70	<3	<3	-	-
IL-1β	3.0 ± 0.9	6.1 ± 1	↑ 104%	0.0004
IL-1ra	358.0 ± 64	188.6 ± 48	↓ 47%	0.02
IL-6	836.4 ± 150	1547.0 ± 145	↑ 85%	0.002
IL-8	102.4 ± 21	181.4 ± 23	↑ 77%	0.003
Insulin	1127.1 ± 381	3767.1 ± 1673	-	0.99
Leptin	271.1 ± 54	151.4 ± 25	-	0.99
Lipocalin-2	3.0 ± 0.6	4.9 ± 1.4	-	0.1
MSPa	182.3 ± 55	121.1 ± 39	-	0.5
OPG	2309.1 ± 351	1775.1 ± 264	↓ 23%	0.0009
PAI-I	6450.2 ± 1172	1738.6 ± 322	↓ 73%	0.0006
PDGF-BB	<3	<3	-	-
Pepsinogen 1	<27	<27	-	-
Pepsinogen 2	<55	<55	-	-
Procalcitonin	393.7 ± 120	<137	↓ 100%	0.006
RANTES	282.4 ± 98	53.5 ± 15	-	0.1
RBP4	6459.1 ± 751	2739.7 ± 90	↓ 58%	0.0009
Resistin	579.2 ± 203	70.3 ± 21	↓ 89%	0.04
SAA	<137	1816.1 ± 186	↑ 100%	0.0005
TGFβ1	<137	278.4 ± 66	↑ 100%	0.006
TSP-1	>200,000	>200,000	-	0.1
TNF RI	<137	<137	-	-
TNF RII	70.7 ± 7	24.7 ± 4	↓ 65%	0.0006
TNFa	98.8 ± 16	48.1 ± 8	↓ 76%	0.006
VEGF	1593.2 ± 73	979.0 ± 39	↓ 39%	0.0000002

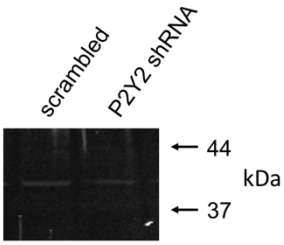

Supplemental figure 1. Representative western blot showing P2Y2 receptor knockdown in adipocytes transduced **Lentivirus *trans* genes encoding scrambled or P2Y2-targeted shRNA**. Loading is normalised by total protein. Black and white image of take using a Li-Cor Biosciences Odyssey infrared scanner. Primary antibody is anti-P2Y2 rabbit polyclonal and secondary is goat anti-rabbit VRDye 490 IgG.